*Article*

# Electrochemical Detection of Cd²⁺, Pb²⁺, Cu²⁺ and Hg²⁺ with Sensors Based on Carbonaceous Nanomaterials and Fe₃O₄ Nanoparticles

Ancuța Dinu (Iacob) [ID], Alexandra Virginia Bounegru [ID], Catalina Iticescu [ID], Lucian P. Georgescu and Constantin Apetrei *[ID]

Department of Chemistry, Physics and Environment, Faculty of Sciences and Environment, "Dunărea de Jos" University of Galati, 47 Domneasca Street, 800008 Galați, Romania; catalina.iticescu@ugal.ro (C.I.); lucian.georgescu@ugal.ro (L.P.G.)
* Correspondence: apetreic@ugal.ro; Tel.: +40-727-580-914

**Abstract:** Two electrochemical sensors were developed in this study, with their preparations using two nanomaterials with remarkable properties, namely, carbon nanofibers (CNF) modified with Fe₃O₄ nanoparticles and multilayer carbon nanotubes (MWCNT) modified with Fe₃O₄ nanoparticles. The modified screen-printed electrodes (SPE) were thus named SPE/Fe₃O₄-CNF and SPE/Fe₃O₄-MWCNT and were used for the simultaneous detection of heavy metals (Cd²⁺, Pb²⁺, Cu²⁺ and Hg²⁺). The sensors have been spectrometrically and electrochemically characterized. The limits of detection of the SPE/Fe₃O₄-CNF sensor were 0.0615 µM, 0.0154 µM, 0.0320 µM and 0.0148 µM for Cd²⁺, Pb²⁺, Cu²⁺ and Hg²⁺, respectively, and 0.2719 µM, 0.3187 µM, 1.0436 µM and 0.9076 µM in the case of the SPE/ Fe₃O₄-MWCNT sensor (following optimization of the working parameters). Due to the modifying material, the results showed superior performance for the SPE/Fe₃O₄-CNF sensor, with extended linearity ranges and detection limits in the nanomolar range, compared to those of the SPE/Fe₃O₄-MWCNT sensor. For the quantification of heavy metal ions Cd²⁺, Pb²⁺, Cu²⁺ and Hg²⁺ with the SPE/Fe₃O₄-CNF sensor from real samples, the standard addition method was used because the values obtained for the recovery tests were good. The analysis of surface water samples from the Danube River has shown that the obtained values are significantly lower than the maximum limits allowed according to the quality standards specified by the United States Environmental Protection Agency (USEPA) and those of the World Health Organization (WHO). This research provides a complementary method based on electrochemical sensors for in situ monitoring of surface water quality, representing a useful tool in environmental studies.

**Keywords:** heavy metals; sensor; square-wave stripping voltammetry; water

## 1. Introduction

In recent years, environmental heavy metal (HM) pollution has increased considerably due to major industrialization in several countries of the world [1–4]. High concentrations of heavy metals can sometimes be found in water, soil, or air, a situation that can lead to serious health problems for vegetation and wildlife, as well as humans [5–8].

Heavy metals are those metallic elements with a density greater than 4.5 g·cm⁻³, such as Cd, Cr, Hg, Pb, Cu or As, all of which are known to have high toxicity, long half-life and non-biodegradability [9–11]. These pollutants come mainly from mining and industrial activities, wastes from mining, smelting, metal refining and coal burning operations [12–14]. When heavy metals enter the environment, they come into direct contact with living organisms and begin to accumulate causing extremely dangerous manifestations such as damage to the digestive, renal, neuronal, cardiovascular, reproductive, visual analyzer systems and even molecular changes in the DNA [15–18]. It is worth mentioning that there are also HMs that are essential for the body and maintenance of health, such as iron, zinc

and copper, but even these can become toxic at high concentrations [19,20]. Therefore, continuous, rapid, sensitive and accurate monitoring of HMs in environmental and food samples is necessary [21–23].

Conventional methods for tracing metal detection at low concentrations include atomic absorption spectroscopy (AAS) [24–27], neutron activation analysis and inductively coupled plasma–optical emission spectrometry (ICP–OES) [28–31], capillary electrophoresis (CE) [32], ion chromatography ultraviolet–visible spectroscopy (IC–UV–Vis) [33,34], inductively coupled plasma mass spectrometry (ICP–MS) [35–39], microwave field hydrothermal method [40,41], X-ray fluorescence spectroscopy (XFS) [42–44], etc. Although these methods have the advantage of high sensitivity and selectivity, there are also some aspects that may limit their use in routine analysis and real-time monitoring of HM ion concentration, such as the high cost of instruments, laborious sample preparation steps, the need for a professional experienced in the application of this technique and laborious preconcentration procedures. Moreover, the equipment is extremely expensive and bulky, which is why it cannot be used for in situ detection [18].

On the other hand, recent research has shown that electrochemical techniques used for heavy metal detection have made significant progress. Recent approaches use electrodes modified with silicon-based materials [45], polymers [46,47], metal nanoparticles [48,49] or carbon-based materials (graphene, carbon nanotubes or carbon nanofibers) [50–52] to enhance the sensitivity and selectivity of HM detection systems. The large surface area, the possibility of functionalization and the extraordinary quantum-mechanical properties of nanomaterials make them suitable and promising for electrode modification. The improved performance of nanomaterial-based sensors comes from the nanoscale electrode surface modification that provides increased catalytic activity, improved conductivity, larger active surface area and very good electrode sensitivity [53–55]. Carbon nanotubes and carbon nanofibers are often used to modify electrodes used in heavy metal detection with excellent results [56–59]. Although both exhibit very good electrocatalytic properties, there are still some differences in terms of shape, size, sensitivity, selectivity and stability that can be amplified or diminished by their functionalization with different nanocomposites, e.g., oxides of transition metals. Transition metal oxides provide a large surface area for the adsorption of analyte molecules to the electrode surface and speed up the charge transfer process. They have higher specific capacitance, high electrical conductivity, higher energy density than carbon materials and better chemical stability. At the same time, carbon-based materials have a large surface with numerous active sites. Also, the carbon matrix acts as a supporting medium for the homogeneous dispersion of nanoparticles, prevents their aggregation and gives a large surface area to volume ratio, enhancing the electrocatalytic process. Carbon matrices are well-known for their large surface area, tensile mechanical strength, rapid rate of electron transfer, exceptionally high electrical and thermal conductivities, which improve the electrochemical process [60,61].

Ferroferric oxide, $Fe_3O_4$ (iron (II, III) oxide), is a material made of magnetic particles with unique properties such as magnetism and chemical reactivity. $Fe_3O_4$ has been widely used in the chemical industry due to its chemical stability, easy preparation, excellent catalytic performance and low toxicity [62–64]. These properties make $Fe_3O_4$ a very useful nanocomposite in various applications, including the functionalization of carbon materials for the detection of heavy metals such as lead, cadmium, mercury and copper. However, due to the high surface energy, $Fe_3O_4$ nanoparticles show a tendency to form aggregates, leading to a significant decrease in active sites [65]. This drawback could be avoided by using a conductive material as a support such as carbon nanotubes or carbon nanofibers, due to their remarkable properties [66]. The introduction of a carbon nanomaterial alongside ferroferric oxide nanoparticles can reduce the formation of $Fe_3O_4$ aggregates, increasing the active surface area available for detection, electron transfer rate and catalytic activity through synergy, and, thus, can improve the detection sensitivity [63].

By using a sensor functionalized with $Fe_3O_4$, efficient detection of heavy metal presence can be achieved through the method of anodic stripping voltammetry. This process

involves modifying the sensor's surface with $Fe_3O_4$ nanoparticles, creating a surface with an affinity for heavy metals. The heavy metals in the solution are then attracted and deposited onto the sensor's surface by applying an appropriate voltage. In the final stage, through the application of a voltammetric method (such as CV, DPV, SWV), the oxidation of the heavy metals on the sensor's surface takes place, leading to an increase in the electric current intensity. This increase is proportional to the initial concentration of heavy metals and provides a sensitive and precise means of detection.

The aim of this study is to investigate the effectiveness and accuracy of electrochemical sensors modified with $Fe_3O_4$ nanoparticles and carbon nanofibers for the simultaneous detection and quantification of heavy metal ions in standard solutions of $Cd^{2+}$, $Pb^{2+}$, $Cu^{2+}$ and $Hg^{2+}$ using square-wave anodic stripping voltammetry. This research adds value to the development of rapid, precise and sensitive methods for detecting heavy metal pollution, with the potential to contribute to environmental monitoring and public health protection.

The novelty of this study resides in the optimized, rapid and easy method of synthesizing $Fe_3O_4$ nanoparticles, utilizing only a few reagents, as well as in the development of new nanocomposites based on carbon nanomaterials. These innovations were utilized to modify two screen-printed electrodes. In this study, the characterization and comparison of two electrochemical sensors modified with $Fe_3O_4$ and carbon nanofibers ($SPE/Fe_3O_4$-CNF) and multilayer carbon nanotubes ($SPE/Fe_3O_4$-MWCNT) were performed on the qualitative and quantitative, simultaneous electrochemical detection of heavy metal ions in standard solutions of the metal ions $Cd^{2+}$, $Pb^{2+}$, $Cu^{2+}$ and $Hg^{2+}$ using square-wave anodic stripping voltammetry. The results are compared with those obtained using the standard addition method to confirm the feasibility of the voltammetric method.

## 2. Materials and Methods

### 2.1. Reagents and Solutions

The supporting electrolyte used for analytical measurements was an acetate buffer solution prepared from sodium acetate and acetic acid purchased from Sigma-Aldrich, St. Louis, MO, USA. The amounts of reagents varied according to the desired pH (4, 4.5, 5, 5.5) and the exact value was determined using the WTW pH meter (Weilheim, Germany). Potassium chloride and potassium ferro- and ferricyanide (Sigma-Aldrich, St. Louis, MO, USA) were used to prepare the solution in which EIS analysis was performed for the characterization of the modified sensors. Multilayer carbon nanotube (MWCNT) powder, carbon nanofibers (CNFs) (Sigma-Aldrich, St. Louis, MO, USA), $FeCl_3 \cdot 6H_2O$ (Carlo Erba Reagents GmbH, Cornaredo, Milan, Italy), ascorbic acid (Sigma-Aldrich, St Louis, MO, USA), hydrazine (LOBA Feinchemie GmbH, Fehrgasse, Austria), ethanol (International Laboratory SRL, Cluj Napoca, Romania), dimethylformamide (DMF) (Sigma-Aldrich, St. Louis, MO, USA) and ultrapure water (obtained with a Milli-Q system—Millipore, Bedford, MA, USA) were used for this study.

The heavy metal salts, $Cu(NO_3)_2$, $(CH_3COO)_2Pb$, $Hg(NO_3)_2$ and $(CH_3COO)_2Cd \cdot 2H_2O$ (Reactiv Plus SRL, Bucharest, Romania), were weighed and solubilized in acetate buffer solution to a concentration of $10^{-4}$ M. Bismuth nitrate (Reactiv Plus SRL, Bucharest, Romania) was then added to the solution for signal optimization at a concentration of 0.3 mg/L.

The actual water samples were taken from the Danube River on the same day from different collection points. Before analysis, the samples were filtered through filter paper to remove possible impurities or visible residues.

### 2.2. Equipment

Electrochemical measurements were carried out using a potentiostat/galvanostat Autolab PGSTAT 302N controlled by Nova 2.1 software, to which an electrochemical cell with a volume of 50 mL was connected. The reference electrode was Ag/AgCl (Princeton, Applied Research), and the auxiliary electrode was platinum wire. The 4 mm diameter screen-printed working electrode was connected to the potentiostat/galvanostat, represented by the modified screen-printed sensors developed in this study. An ultrasonic bath

was used for the dissolution of compounds, homogenization of solutions and dispersion of nanoparticles and nanofibers. To characterize the modified sensors and validate the results, FT-IR measurements in attenuated total reflectance (ATR) mode were performed. The ATR crystal made of ZnSe was cleaned with ultrapure water and isopropanol after each measurement. Buffer solutions were adjusted to the desired pH using a glass pH electrode connected to a WTW pH meter (Weilheim, Germany). Cencom II centrifuge was used in the separation process of $Fe_3O_4$-MWCNT and $Fe_3O_4$-CNF nanocomposites.

### 2.3. Synthesis of $Fe_3O_4$-MWCNT and $Fe_3O_4$-CNF Nanocomposites

In the first step, $Fe_3O_4$ nanoparticles were synthesized using a mixture consisting of 0.3 g $FeCl_3 \cdot 6H_2O$, 0.5 g ascorbic acid, 10 mL hydrazine and 50 mL ultrapure distilled water. The mixture was dried in the oven for 8 h at 180 °C. During the 8 h, the mixture was rinsed twice with ethanol and water. In the second step, 25 mg $Fe_3O_4$ and 100 mg MWCNT or CNF were dispersed in 10 mL ethanol and centrifuged for 5 min, then dried at 150 °C for 2 h.

While the synthesis process was carefully controlled to ensure the formation of $Fe_3O_4$ nanoparticles, the focus of this research was on the development and application of nanocomposites and the synthesis method for $Fe_3O_4$ nanoparticles was based on established protocols [67,68].

### 2.4. Construction of Electrochemical Sensors

The suspension with catalytic properties was prepared by dispersing 10 mg $Fe_3O_4$-MWCNT, $Fe_3O_4$-CNF mixture in 500 μL water and dimethylformamide in a 1:1 ratio. The mixture was sonicated for 30 min for good homogenization. A volume of 10 μL was deposited on the SPE surface by the drop-casting technique in two steps with a drying break of 1 h. The added suspension volume was optimized. For the preliminary analyses, MWCNT-only and CNF-only screen-printed sensors were also constructed using the same technique and suspension volume. All modified sensors were kept at room temperature. The steps in the SPE/$Fe_3O_4$-CNF sensor construction are schematically represented in Figure 1.
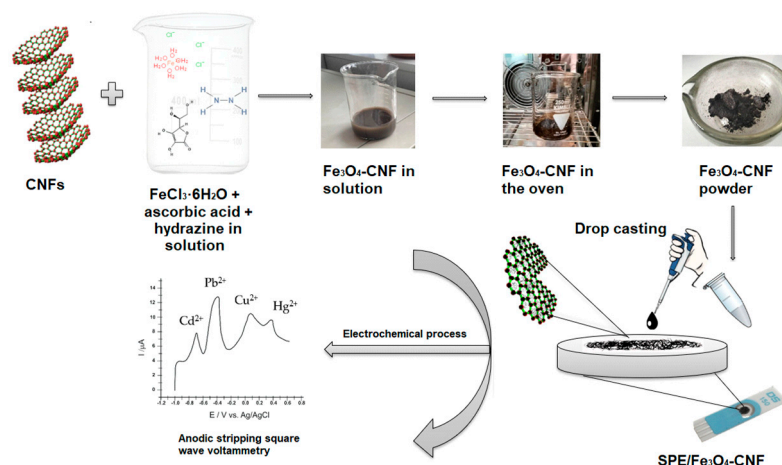


**Figure 1.** Scheme of the SPE/$Fe_3O_4$-CNF fabrication.

### 2.5. Methods of Analysis

Electrochemical methods (electrochemical impedance spectroscopy) and spectrometric methods (Fourier transform infrared spectroscopy) were used to characterize the modified sensors. The electrochemical behavior of the modified sensors in an aqueous solution with $K_4[Fe(CN)_6]$ $10^{-3}$ M and KCl $10^{-1}$ M was evaluated by cyclic voltammetry (CV). Square-wave anodic stripping voltammetry (SWASV) was employed for the detection of heavy metal ions, their calibration curve and quantification in real samples.

### 2.6. Statistical Data Processing Methodology

Various statistical data processing techniques were employed for the analysis and interpretation of data obtained from the electrochemical study and for evaluating the performance of the developed sensors. These techniques include linear regression, calculation of standard deviation, recovery calculation, coefficient of variation and interpretation of the obtained electrochemical parameters. Excel software (version 2401) and the Data Analysis Toolbox were utilized for the statistical analysis of these data.

## 3. Results and Discussion

### 3.1. Characterization of the Modified Surface

Electrochemical impedance spectroscopy (EIS) was used to characterize the modified active surface of the new electrochemical sensors. This technique is based on measuring the electrical impedance of an electrochemical cell as a function of frequency when an alternating voltage is applied. EIS can provide information about the electrochemical properties of the modified surface, such as resistance, capacitance and the kinetics of electron transfer, but it does not directly provide information about the sensitivity and selectivity of an electrode, which are analytical parameters.

In this case, the electrochemical processes taking place at the interface of the modified working electrodes and the electrolyte chosen for analysis (in this case, $10^{-3}$ M $K_3[Fe(CN)_6]/K_4[Fe(CN)_6]$ and $10^{-1}$ M KCl in a 1:1 ratio) were fitted using an equivalent circuit involving resistors, capacitors and inductors. The Randles equivalent circuit is a commonly used model in electrochemical impedance spectroscopy to represent the electrochemical processes occurring at the electrode interface. It shows, in a simplified way, the solution resistance ($R_s$), the capacitance of the double layer at the electrode surface ($C_{dI}$), the charge transfer resistance ($R_{ct}$) and the Warburg resistance ($Z_w$) [69]. According to Figure 2, the Nyquist diagrams obtained in this study (in the form of a semicircle) correspond to a simulated Randles circuit.
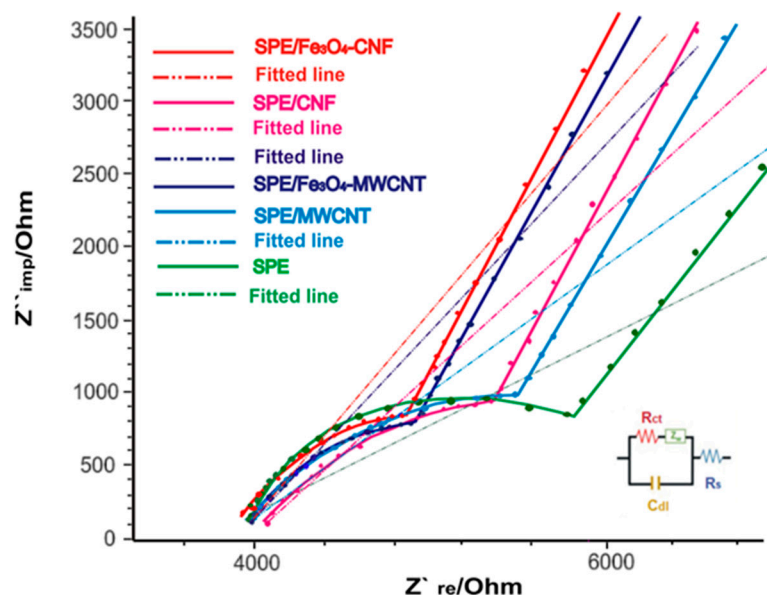


**Figure 2.** Nyquist plots of EIS and fitted line for SPE/Fe$_3$O$_4$-CNF (red line), SPE/CNF (pink line), SPE/Fe$_3$O$_4$-MWCNT (dark blue line), SPE/MWCNT (blue line) and SPE (green line) in $10^{-1}$ M KCl and $10^{-3}$ M $[Fe_4(CN)_6]^{3-/4-}$ for a frequency range of 0.1 Hz to $10^6$ Hz, amplitude 5 mV. Inset: Equivalent circuit is applied to fit the impedance spectra.

In the case of modified sensors, the electron transfer resistance ($R_{ct}$) is being evaluated, with a higher value indicating lower conductivity. The presence of the Fe$_3$O$_4$ nanoparticles leads to lower electron transfer resistance and, thus, better electrocatalytic properties. As

expected, the $R_{ct}$ value was 5353.7 $\Omega$ for the SPE/CNF electrode, and, for the SPE/Fe$_3$O$_4$-CNF, it decreases to a value of 4849.2 $\Omega$. The same behavior is observed for SPE/MWCNT (5505.67 $\Omega$) and SPE/Fe$_3$O$_4$-MWCNT (4858.16 $\Omega$). $R_{ct}$ values of the modified sensors are lower than that of the unmodified screen-printed electrode (SPE) ($R_{ct}$ = 5805 $\Omega$). It is worth mentioning that SPE/Fe$_3$O$_4$-CNF has the lowest value of electron transfer resistance, so it can be assumed that the structure and size of carbon nanofibers, together with Fe$_3$O$_4$ nanoparticles, enhance their electrical properties, favoring a more sensitive detection.

FT-IR spectroscopy was used to evaluate the main functional groups present in the four composite nanomaterials deposited on the screen-printed electrodes (Figure 3). The characteristic vibrational stretching associated with Fe-O bonds, where Fe$_3$O$_4$ nanoparticles exist, is observed at wavelengths 585 and 640 cm$^{-1}$ in the case of SPE/Fe$_3$O$_4$-MWCNT, respectively, at 560 and 625 cm$^{-1}$ in the case and SPE/Fe$_3$O$_4$-CNF. These bands correspond to Fe-O (Fe (II) and/or Fe (III)) in octahedral and tetrahedral geometries, as mentioned in the literature [70]. In all four spectra, bending vibrations in the range 1500–1700 cm$^{-1}$ and stretching vibrations in the range 3250–3300 cm$^{-1}$ of the O-H groups occur. Finally, the existence of carbonaceous nanomaterials is inferred by the C-H stretching bands between 2850–2925 cm$^{-1}$ and the vibrations of the C-C and C-N groups in the range 1200–1500 cm$^{-1}$.
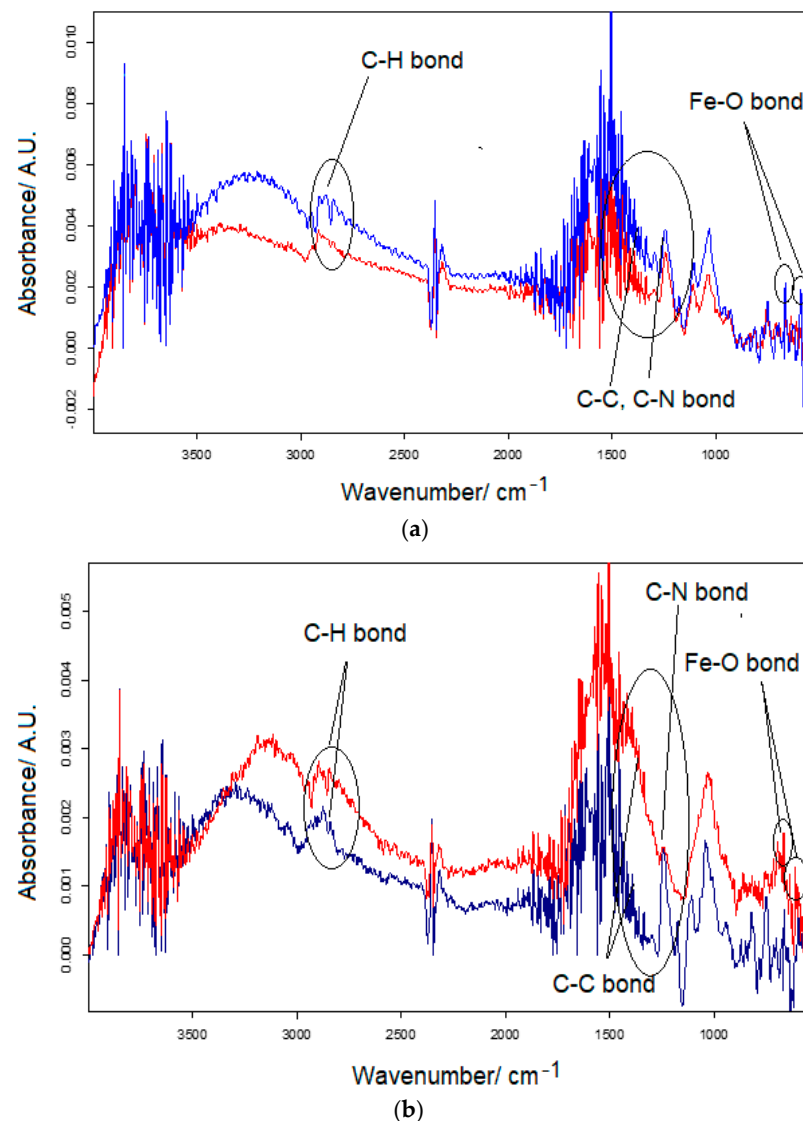


**Figure 3.** FT-IR spectra for (**a**) SPE/CNF (red line), SPE/Fe$_3$O$_4$-CNF (blue line), and (**b**) SPE/Fe$_3$O$_4$-MWCNT (blue line).

### 3.2. Electrochemical Behavior of SPE/Fe$_3$O$_4$-MWCNT and SPE/Fe$_3$O$_4$-CNF in Potassium Ferrocyanide Solution

An intriguing observation in our study pertains to the electrochemical behavior of the MWCNTs composite compared to CNFs. Despite the higher intrinsic conductivity of MWCNTs, the composite exhibited lower electron transfer kinetics and surface area. Several factors contribute to this behavior. Firstly, the nature of the interaction between MWCNTs and Fe$_3$O$_4$ nanoparticles may differ from that with CNFs, affecting the overall conductivity of the composite. Secondly, the dispersion quality of MWCNTs in the composite may be different from that of CNFs. Any aggregation can reduce the effective surface area and hinder electron transfer. Thirdly, structural variations between MWCNTs and CNFs, such as the number of layers, alignment and defects, can lead to differences in electron transfer kinetics and surface area. Lastly, the performance of the composite is influenced by the synergistic effects of its components. The combination of Fe$_3$O$_4$ with CNFs may result in a more favorable synergy for electron transfer compared to the combination with MWCNTs. This detailed analysis provides insights into the complex behavior of the CNFs composite and enhances our understanding of its electrochemical properties in comparison to MWCNTs.

The electrochemical behavior of SPE bare and the four modified sensors (SPE/MWCNT, SPE/CNF, SPE/Fe$_3$O$_4$-MWCNT, SPE/Fe$_3$O$_4$-CNF) was studied in a solution of K$_4$[Fe(CN)$_6$] $10^{-3}$ M-KCl $10^{-1}$ M. The potential range was between $-0.4$ and $+1.0$ V, and the scan rate was $0.1$ V·s$^{-1}$. Figure 4 shows the redox process of potassium ferrocyanide, well-highlighted with each electrode. Oxidation and reduction peaks are present in each situation, proving a quasi-reversible redox process. However, the intensity and potential of the peaks are slightly different depending on the sensor used, which shows the differences imprinted by the modifications of the active surface.
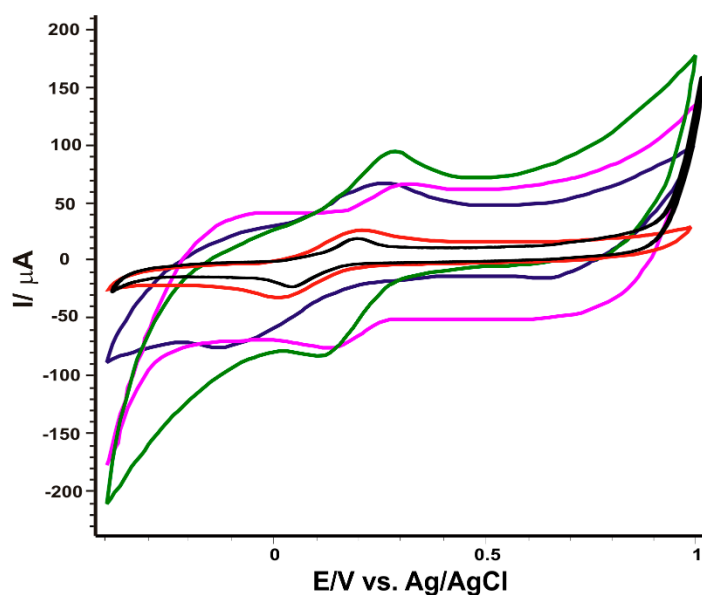


**Figure 4.** The cyclic voltammograms of SPE (black line), SPE/CNF (red line), SPE/Fe$_3$O$_4$-CNF (green line), SPE/MWCNT (violet line) and SPE/Fe$_3$O$_4$-MWCNT (blue line) immersed in K$_4$[Fe(CN)$_6$] $10^{-3}$ M-KCl $10^{-1}$ M solution. Scan rate $0.1$ V·s$^{-1}$.

As can be seen in Table 1, all modified sensors show a value of the ratio $I_{pc}/I_{pa}$ very close to 1, indicating optimal peak reversibility. Although the oxidation peak intensities of SPE/MWCNT and SPE/Fe$_3$O$_4$-MWCNT sensors have very close values, the latter exhibits a lower oxidation potential, suggesting better selectivity, likely due to the presence of Fe$_3$O$_4$ nanoparticles on the active surface of SPE/Fe$_3$O$_4$-MWCNT. On the other hand, SPE/Fe$_3$O$_4$-CNF shows the highest peaks, an $I_{pc}/I_{pa}$ ratio close to 1 and an optimal $E_{1/2}$ value (fairly close to the theoretical $E_{1/2}$ value ($0.36$ V) obtained from the hydrogen elec-

trode in the $[Fe(CN)_6]^{4-}$-$[Fe(CN)_6]^{3-}$ redox process [71]), suggesting favorable dynamics of the redox process. The slightly lower value of $\Delta E$ obtained by the SPE/Fe$_3$O$_4$-CNF sensor suggests faster kinetics and improved reversibility of the redox process at the electrode interface. While the difference in performance between the modified SPE/CNF and SPE/Fe$_3$O$_4$-CNF sensors, and between SPE/MWCNT and SPE/Fe$_3$O$_4$-MWCNT, may not be substantial, it is noteworthy. The attachment of colloidal particles on a given surface and their interaction is a complex process, dependent on several parameters such as surface chemical processes, colloidal particle size, presence of ligands and type of dispersant [72]. Therefore, the observed variations in electrochemical response can be attributed to differences in the interaction between Fe$_3$O$_4$ and CNFs, influenced by the size and shape of CNFs and the resulting synergistic effects between nanocomposites. To calculate the active surface area of the modified sensors, the kinetics of the redox process of $10^{-3}$ M potassium ferrocyanide–$10^{-1}$ M KCl was studied by applying several scanning rates (0.1–0.5 V·s$^{-1}$). Following the measurements, a linear dependence between the intensity of the oxidation peak and the square of the scan rate is found in each case. This result shows that the electrochemical process is controlled by the diffusion of the ferrocyanide ion at the surface of the working electrode. Therefore, knowing the diffusion coefficient of K$_4$[Fe(CN)$_6$] ($7.26 \times 10^{-6}$ cm$^2$·s$^{-1}$ [73], from the Randles–Sevcik equation [74], the active surface areas of the four sensors were found, and the values are shown in Table 2.

**Table 1.** Main electrochemical parameters obtained from voltammograms of sensors immersed in an aqueous solution with K$_4$[Fe(CN)$_6$] $10^{-3}$ M and KCl $10^{-1}$ M.

| Electrode | $E_{pa}$ [1] (V) | $E_{pc}$ [2] (V) | $E_{1/2}$ [3] (V) | $I_{pa}$ [4] (µA) | $I_{pc}$ [5] (µA) | $\Delta E$ [6] | $I_{pc}/I_{pa}$ |
|---|---|---|---|---|---|---|---|
| SPE | 0.201 | 0.045 | 0.123 | 19.85 | −24.35 | 0.156 | 1.22 |
| SPE/CNF | 0.195 | 0.015 | 0.105 | 25.67 | −30.85 | 0.180 | 1.20 |
| SPE/MWCNT | 0.300 | 0.135 | 0.217 | 61.75 | −71.08 | 0.165 | 1.15 |
| SPE/Fe$_3$O$_4$-CNF | 0.274 | 0.126 | 0.200 | 94.11 | −83.89 | 0.148 | 0.89 |
| SPE/Fe$_3$O$_4$-MWCNT | 0.265 | −0.126 | 0.195 | 62.11 | −74.78 | 0.391 | 1.20 |

[1] potential of the anodic peak; [2] potential of the cathodic peak; [3] half-wave potential; [4] current of the anodic peak; [5] current of the cathodic peak; [6] $\Delta E = E_{pa} - E_{pc}$.

**Table 2.** $I_{pa}$ vs. $v^{1/2}$ and log $I_{pa}$ vs. log $v$ linear regression equations, $R^2$, geometrical areas, active surface areas and the roughness factors of all the modified SPEs studied.

| Electrode | Linear Equation $I_{pa}$ vs. $v^{1/2}$ | $R^2$ | Linear Equation log $I_{pa}$ vs. log $v$ | $R^2$ | Points | Geometric Area (cm$^2$) | Active Area (cm$^2$) | Roughness Factor |
|---|---|---|---|---|---|---|---|---|
| SPE | I (A) = $6.64 \times 10^{-5}$ $v^{1/2}$ (V·s$^{-1}$)$^{1/2}$ + $4.61 \times 10^{-6}$ | 0.9861 | log $I_{pa}$ = 0.4614 log $v$ − 4.1402 | 0.9865 | | | 0.032 | 0.25 |
| SPE/CNF | I (A) = $7.79 \times 10^{-5}$ $v^{1/2}$ (V·s$^{-1}$)$^{1/2}$ + $1.85 \times 10^{-6}$ | 0.9972 | log $I_{pa}$ = 0.4891 log $v$ − 4.0953 | 0.9975 | | | 0.039 | 0.31 |
| SPE/MWCNT | I (A) = $1.77 \times 10^{-4}$ $v^{1/2}$ (V·s$^{-1}$)$^{1/2}$ + $8.83 \times 10^{-6}$ | 0.9893 | log $I_{pa}$ = 0.4688 log $v$ − 3.7283 | 0.9905 | 5 | 0.125 | 0.086 | 0.69 |
| SPE/Fe$_3$O$_4$-CNF | I (A) = $5.43 \times 10^{-4}$ $v^{1/2}$ (V·s$^{-1}$)$^{1/2}$ + $7.78 \times 10^{-5}$ | 0.9999 | log $I_{pa}$ = 0.7341 log $v$ − 3.282 | 0.9972 | | | 0.265 | 2.12 |
| SPE/Fe$_3$O$_4$-MWCNT | I (A) = $3.72 \times 10^{-4}$ $v^{1/2}$ (V·s$^{-1}$)$^{1/2}$ + $5.35 \times 10^{-5}$ | 0.9979 | log $I_{pa}$ = 0.7524 log $v$ − 3.4367 | 0.9914 | | | 0.181 | 1.44 |

It can be seen in Table 2 that the active surface area increases significantly after the addition of Fe$_3$O$_4$ in the modifying nanocomposite material, especially in the case of SPE/Fe$_3$O$_4$-CNF, where the roughness factor is 2.12.

Nevertheless, through the analysis of the log(I) vs. log(v) graphs for the modified electrodes, a broader perspective emerges regarding the influence of chemical interactions in the redox process of potassium ferrocyanide. The slope values of 0.73 for SPE/Fe$_3$O$_4$-CNF and 0.75 for SPE/Fe$_3$O$_4$-MWCNT indicate significant deviations from the theoretical model (0.5) [75], suggesting a pronounced influence of chemical species in the redox reaction for both modified electrodes. This underscores their enhanced efficiency in capturing

and recognizing redox species, thereby facilitating further applications in sensitive and selective analytical detection. The subtle differences in slope values between the two types of electrodes can be attributed to specific surface variations.

Since the addition of $Fe_3O_4$ nanoparticles helped to improve the responses in the preliminary studies and the nanocomposite showed up on the active surface of the electrodes by both FT-IR and EIS methods, only the modified $SPE/Fe_3O_4$-CNF and $SPE/Fe_3O_4$-MWCNT sensors were used for heavy metal ion detection studies.

### 3.3. Electrochemical Detection of Heavy Metals Using SPE/Fe₃O₄-MWCNT and SPE/Fe₃O₄-CNF

Square-wave anodic stripping voltammetry (SWASV) involves applying a variable voltage to the working electrode that varies rapidly between two values. This potential variation leads to a variation in electric current, which can be measured and recorded. This is because heavy metals deposited on the surface of the electrode have a tendency to oxidize at the anode, leading to an increase in the electric current. The magnitude of the electric current depends on the concentration of heavy metals in the solution [76,77].

A stock solution of $Cd^{2+}$, $Hg^{2+}$, $Cu^{2+}$ and $Pb^{2+}$ in equal concentrations of $10^{-4}$ M in $10^{-1}$ M acetate buffer solution was prepared for heavy metal detection analysis.

After immersion of the electrode in the stock solution, parameters were set for the electrodeposition step, for square-wave voltammetry measurements, and for the desorption step of heavy metals from the surface of the working electrodes.

In Figure 5, the presence of each metal ion can be seen through a well-highlighted peak at different potentials, in accordance with literature data [63].
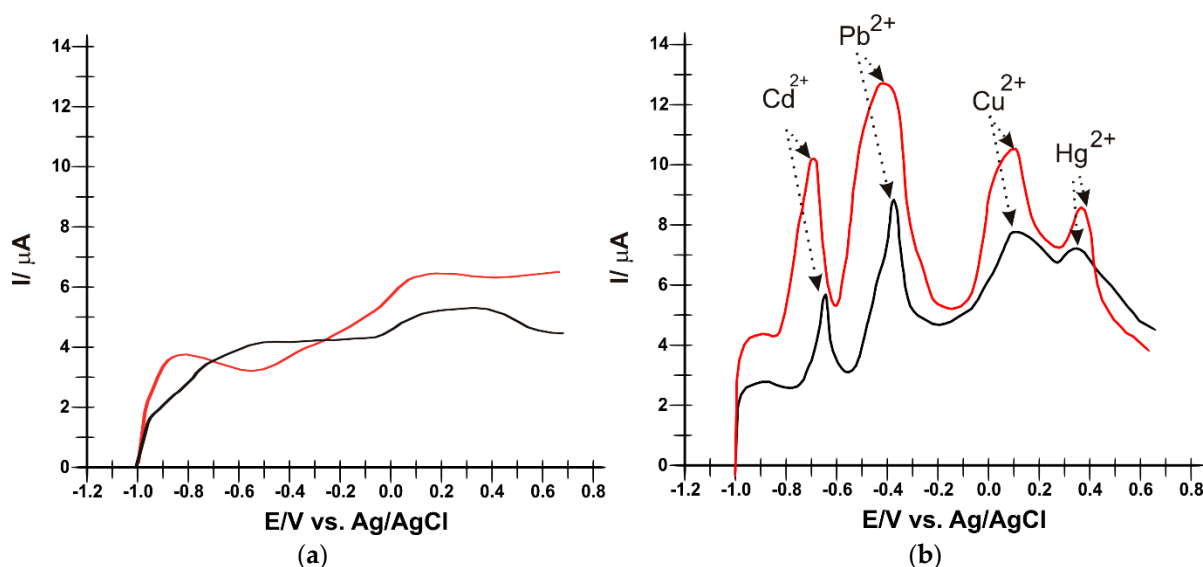


**Figure 5.** SWASV of $SPE/Fe_3O_4$-CNF (red line) and $SPE/Fe_3O_4$-MWCNT (black line) in (**a**) $10^{-1}$ M acetate buffer solution (pH 5.0) and (**b**) $10^{-1}$ M acetate buffer solution (pH 5.0) containing $10^{-4}$ M of $Cd^{2+}$, $Pb^{2+}$, $Cu^{2+}$ and $Hg^{2+}$. Parameters applied: f (frequency) = 25 Hz; $E_{sw}$ (applied pulse) = 20 V, $E_i$–$E_f$ (applied potential range) = $-1.0$–0.6 V. Electrodeposition parameters: E = $-1.2$ V for 180 s; Desorption parameters: E = 1 V for 210 s.

The electrochemical behavior of heavy metal ions has been thoroughly investigated using SWASV. Peaks are well-defined with low background noise. The recorded voltammograms demonstrate that Cd, Pb, Cu and Hg ions can be identified and quantified by this voltammetric method. The electrochemical parameters obtained with $SPE/Fe_3O_4$-CNF and $SPE/Fe_3O_4$-MWCNT by applying SWASV are presented in Table 3.

**Table 3.** The values of the parameters obtained from square-wave voltamograms of SPE/Fe$_3$O$_4$-CNF and SPE/Fe$_3$O$_4$-MWCNT in $10^{-4}$ M metallic ions (the electrolyte support was $10^{-1}$ M acetate buffer at pH 5.0).

| Electrode | Metallic Ion | $E_{pa}$ (V) | $I_{pa}$ (μA) |
|---|---|---|---|
| **SPE/Fe$_3$O$_4$-CNF** | Cd$^{2+}$ | −0.696 | 10.150 |
| | Pb$^{2+}$ | −0.423 | 12.681 |
| | Cu$^{2+}$ | 0.106 | 10.607 |
| | Hg$^{2+}$ | 0.362 | 8.581 |
| **SPE/Fe$_3$O$_4$-MWCNT** | Cd$^{2+}$ | −0.648 | 5.545 |
| | Pb$^{2+}$ | −0.374 | 8.783 |
| | Cu$^{2+}$ | 0.092 | 7.670 |
| | Hg$^{2+}$ | 0.341 | 7.213 |

It can be seen from Table 3 that all the peaks corresponding to heavy metals in the solution have a higher intensity and are better defined when SPE/Fe$_3$O$_4$-CNF was used for detection compared to SPE/Fe$_3$O$_4$-MWCNT. This may be due to the higher affinity of Fe$_3$O$_4$ nanoparticles for CNFs and, therefore, a better sensitivity for heavy metals that are present in the solution. The $E_{pa}$ values constitute crucial aspects in electrochemical analysis, signifying the preferred moments for oxidation reactions at the electrode surface. In the context of the presented research, a diversity of $E_{pa}$ values for various metal ions on SPE/Fe$_3$O$_4$-CNF and SPE/Fe$_3$O$_4$-MWCNT electrodes has been highlighted.

The negative $E_{pa}$ values for ions such as Cd$^{2+}$ and Pb$^{2+}$ indicate a propensity towards oxidation at lower potentials, while the positive values associated with Cu$^{2+}$ and Hg$^{2+}$ denote oxidation processes occurring at higher potentials. These variations can be attributed to structural differences in metal ions and interactions with electrode surfaces. The slight differences between the electrodes can be explained by the distinctions in the structural materials employed. It is important to emphasize that the $E_{pa}$ values are congruent with the conclusions of previous studies, underscoring the consistency of experimental choices [63].

*3.4. Optimization of Working Parameters*

In the next step, optimization studies of the working parameters, namely, the influence of bismuth ions in the electrochemical response, the pH of the solution and the deposition time, were carried out.

As shown in Figure 6a,b, the current intensities corresponding to each metal ion in the solution, recorded with the SPE/Fe$_3$O$_4$-CNF and SPE/Fe$_3$O$_4$-MWCNT sensors in the presence of 0.3 mg/L Bi$^{3+}$, showed a slight increase in peak intensity for all metal ions, but also more stable signals regarding consistency and predictability over time, along with reduced background noise. When a lower concentration (0.2 mg/L) was introduced, improvements in signal fidelity were observed for only two of the metal ions (Cd$^{2+}$ and Pb$^{2+}$); consequently, the decision was made to use a higher concentration.

Specific interactions between the Bi$^{3+}$ ion and the electrode surfaces can facilitate oxidation reactions associated with heavy metal ions. Additionally, signal stabilization could result from a positive influence of Bi$^{3+}$ ions on the kinetics of electrochemical processes, thereby enhancing signal reproducibility. These are confirmed by calculating the standard deviation of the intensity values corresponding to heavy metal peaks in the presence and absence of Bi$^{3+}$ (five recorded cyclic voltammograms) for both newly developed sensors, and the results are detailed in Table 4. This result indicates that bismuth could significantly improve the analytical performance by forming a "molten alloy" with the target metals, thus facilitating the redox process at the electrode surface [52]. Thus, both modified sensors in the presence of Bi$^{3+}$ had improved sensitivity.
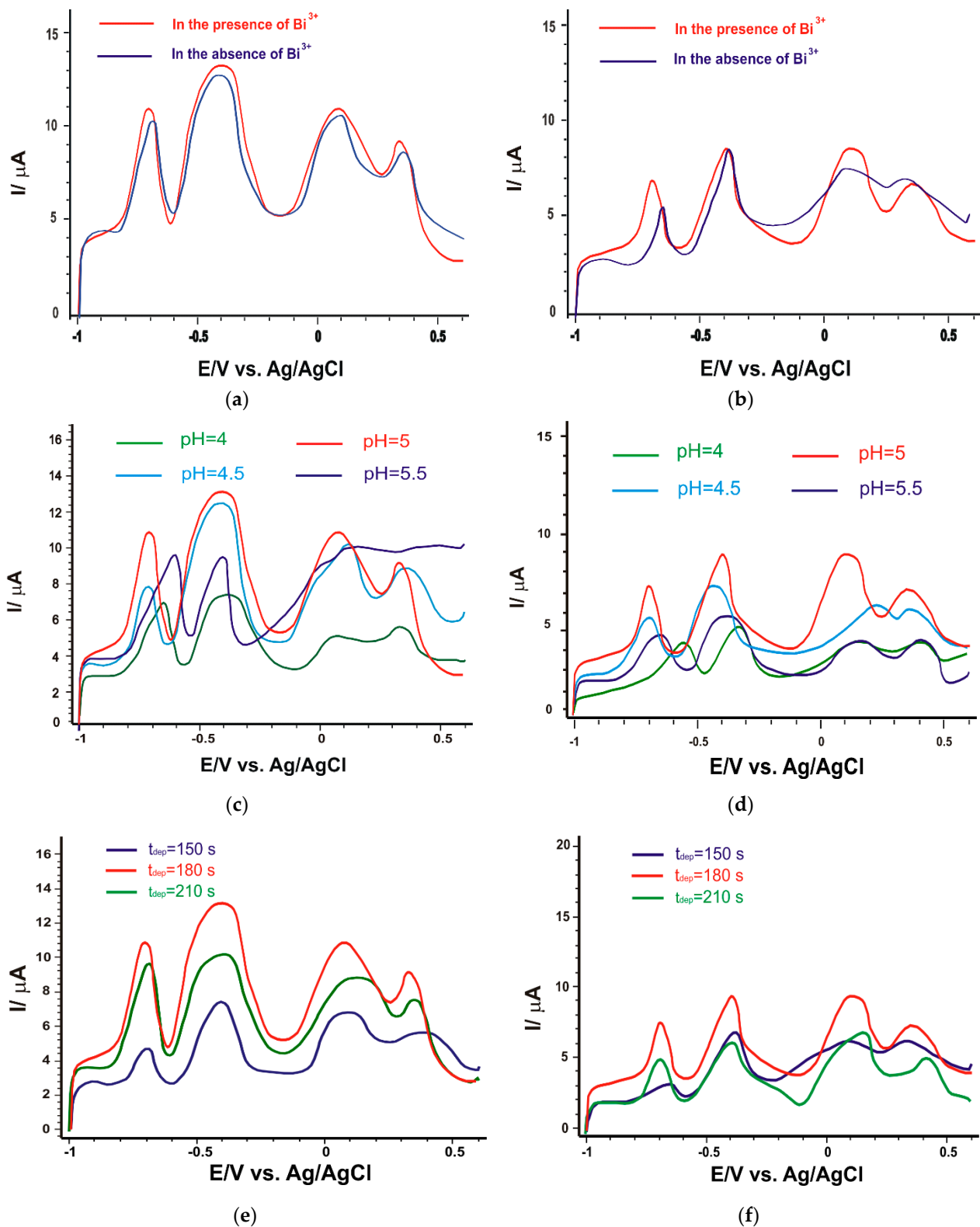
**Figure 6.** SWASV of the sensor (**a**) SPE/Fe$_3$O$_4$-CNF and (**b**) SPE/Fe$_3$O$_4$-MWCNT in $10^{-4}$ M heavy metal stock solution (of each metal ion) in the presence (red line) and absence of Bi (blue line); SWASV of the sensor (**c**) SPE/Fe$_3$O$_4$-CNF and (**d**) SPE/Fe$_3$O$_4$-MWCNT in the presence of Bi immersed in heavy metal stock solution at different pH values; SWASV of the sensor (**e**) SPE/Fe$_3$O$_4$-CNF and (**f**) SPE/Fe$_3$O$_4$-MWCNT in the presence of Bi immersed in heavy metal stock solution using different deposition times.

**Table 4.** Standard deviations of peak intensities for heavy metals in the presence and absence of $Bi^{3+}$ for SPE/$Fe_3O_4$-CNF and SPE/$Fe_3O_4$-MWCNT.

| | σ (Standard Deviation) | | | | | | | |
|---|---|---|---|---|---|---|---|---|
| | $Cd^{2+}$ | | $Pb^{2+}$ | | $Cu^{2+}$ | | $Hg^{2+}$ | |
| Sensor | In Presence of $Bi^{3+}$ | In Absence of $Bi^{3+}$ | In Presence of $Bi^{3+}$ | In Absence of $Bi^{3+}$ | In Presence of $Bi^{3+}$ | In Absence of $Bi^{3+}$ | In Absence of $Bi^{3+}$ | In Absence of $Bi^{3+}$ |
| SPE/$Fe_3O_4$-CNF | 0.00376 | 0.00646 | 0.00415 | 0.01870 | 0.00178 | 0.00719 | 0.00788 | 0.01036 |
| SPE/$Fe_3O_4$-MWCNT | 0.00618 | 0.01 | 0.00291 | 0.01045 | 0.00364 | 0.00828 | 0.00985 | 0.01848 |

Next, the effect of pH on the current strengths in the heavy metal-containing stock solution was studied. During electrodeposition, there is a local increase in pH at the electrode surface that should not be neglected; therefore, the pH value of the buffer solution should be optimized. In this study, four pH values were studied: 4, 4.5, 5 and 5.5. According to the literature, in the application of the SWASV technique, the optimal pH range of the acetate buffer solution is 4–5.6 [76].

As can be seen in Figure 6b,c, there is a considerable difference between the appearance of the voltammograms at the four pH values. The lower pH value resulted in currents of much lower intensity, possibly due to the protonation of the hydrophilic groups of the carbon nanofibers [78]. With increasing pH (4.5 and 5), the currents increased progressively, with a slight decrease when the pH of the solution was 5.5 (Figure 7a). The decrease in current intensity was probably due to the formation of metal complexes [78]. This behavior was observed for both sensors. In the case of the SPE/$Fe_3O_4$-CNF sensor, at pH = 5.5, although the $Cd^{2+}$ and $Pb^{2+}$ peaks are well-defined, the signal loses stability and the presence of $Cu^{2+}$ and $Hg^{2+}$ is no longer evident. Also, the potential at which heavy metal oxidation peaks occur is lower when the pH value is 5, which contributes to better sensor sensitivity. A lower potential at which oxidation peaks occur can enhance the oxidation reactions of heavy metal ions, leading to a more pronounced electrochemical signal generation, thereby contributing to improved sensor sensitivity. It is therefore considered that pH 5 is optimal for the simultaneous determination of the four heavy metal ions.

Finally, the effect of deposition time was investigated, as shown in Figure 6d,e. The current intensities increased significantly when the deposition time changed from 150 s to 180 s. However, at a longer deposition time of 210 s, the current intensity decreased obviously. This behavior may be due to a saturation effect for the bismuth film and the amount of heavy metal ions on the electrode surface. Thus, 180 s was selected as the optimal deposition time.

In Figure 7, the graphs illustrate both the relationship between pH and current intensities, as well as the dependence between pH and the potential associated with metal ions for the two modified sensors.
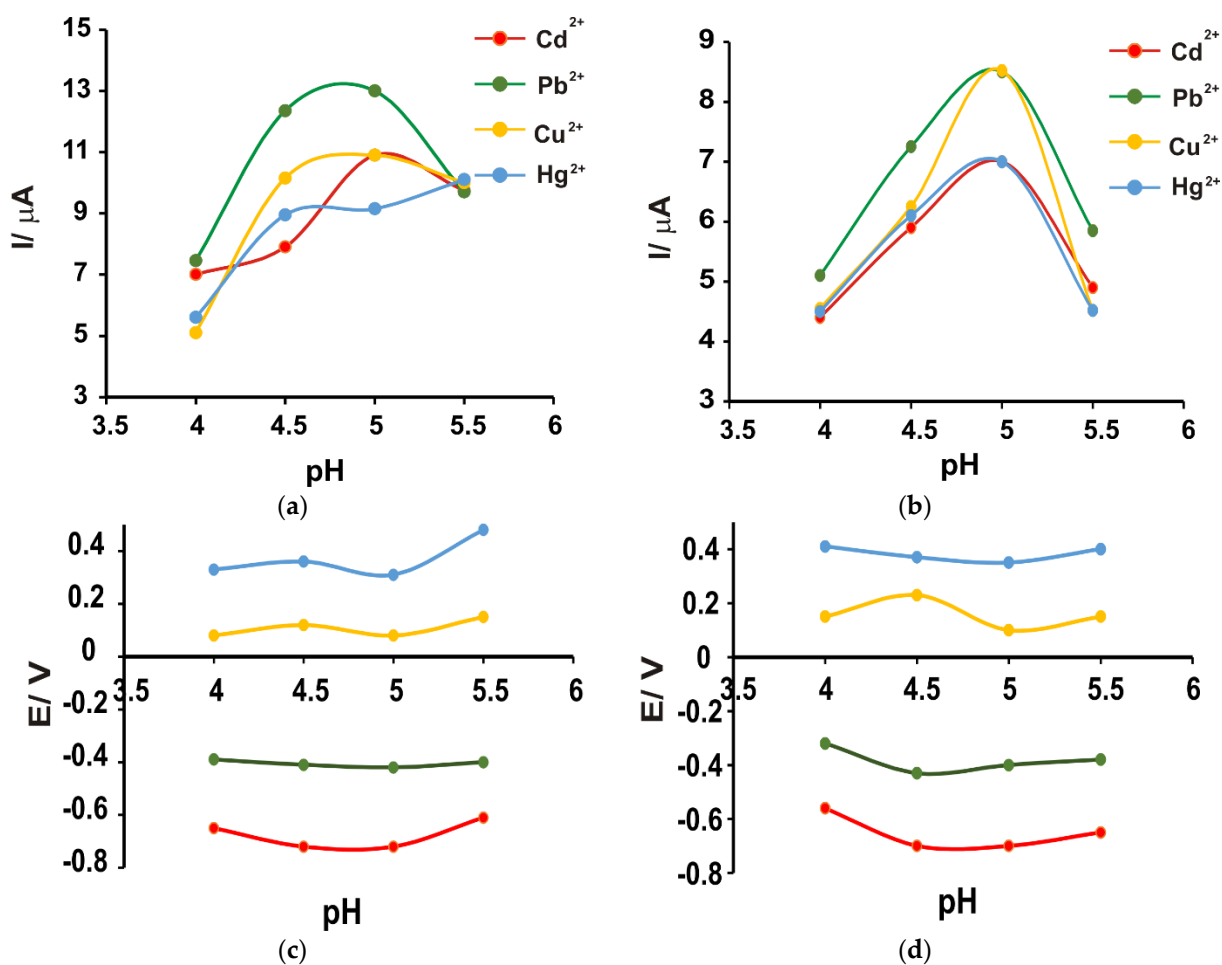
**Figure 7.** The dependence between pH and the peak currents related to the presence of metal ions in the case of (**a**) SPE/Fe$_3$O$_4$-CNF and (**b**) SPE/Fe$_3$O$_4$-MWCNT. The relationship between pH and the potential associated with the presence of a metal ion is depicted for (**c**) SPE/Fe$_3$O$_4$-CNF and (**d**) SPE/Fe$_3$O$_4$-MWCNT configurations.

*3.5. The Electrochemical Responses of the SPE/Fe$_3$O$_4$-CNF and SPE/Fe$_3$O$_4$-MWCNT Sensors in Solutions of Different Concentrations*

The study continued with the realization of the calibration curves, this being an important step for the characterization of the developed voltammetric method, calculating the limits of detection (LOD) and quantification (LOQ) for each electrochemical sensor. Thus, the SWASV method was used for all electrodes modified for the detection and subsequent quantification of heavy metal ions Cd$^{2+}$, Pb$^{2+}$, Cu$^{2+}$ and Hg$^{2+}$ using the same working parameters as in the previous stage, i.e., the presence of bismuth ions, pH 5, adsorption potential and time (E = −1.2 V, time 180 s), desorption potential and time (E = 1 V, time 210 s). The concentration range studied was 0.5–80 μM. The solutions for making the calibration curve were obtained by mixing different volumes of 10$^{-4}$ M heavy metal stock solution added in an acetate buffer solution.

Figure 8a,b shows the voltammograms obtained in standard solutions containing heavy metal ions, of different concentrations, in the 0.5–80 μM range, and Figure 8c,d shows a linear dependence between the intensity of the anodic peaks and the concentration of each metal ion in the solution to be analyzed, both for SPE/Fe$_3$O$_4$-CNF and for SPE/Fe$_3$O$_4$-MWCNT. However, superior analytical performances were obtained with the SPE/Fe$_3$O$_4$-CNF sensor, which shows increased anodic peak intensities compared to the SPE/Fe$_3$O$_4$-MWCNT sensor, due to the increased compatibility of nanoparticles for CNFs, but especially for heavy metal ions, to which the sensitivity is higher.
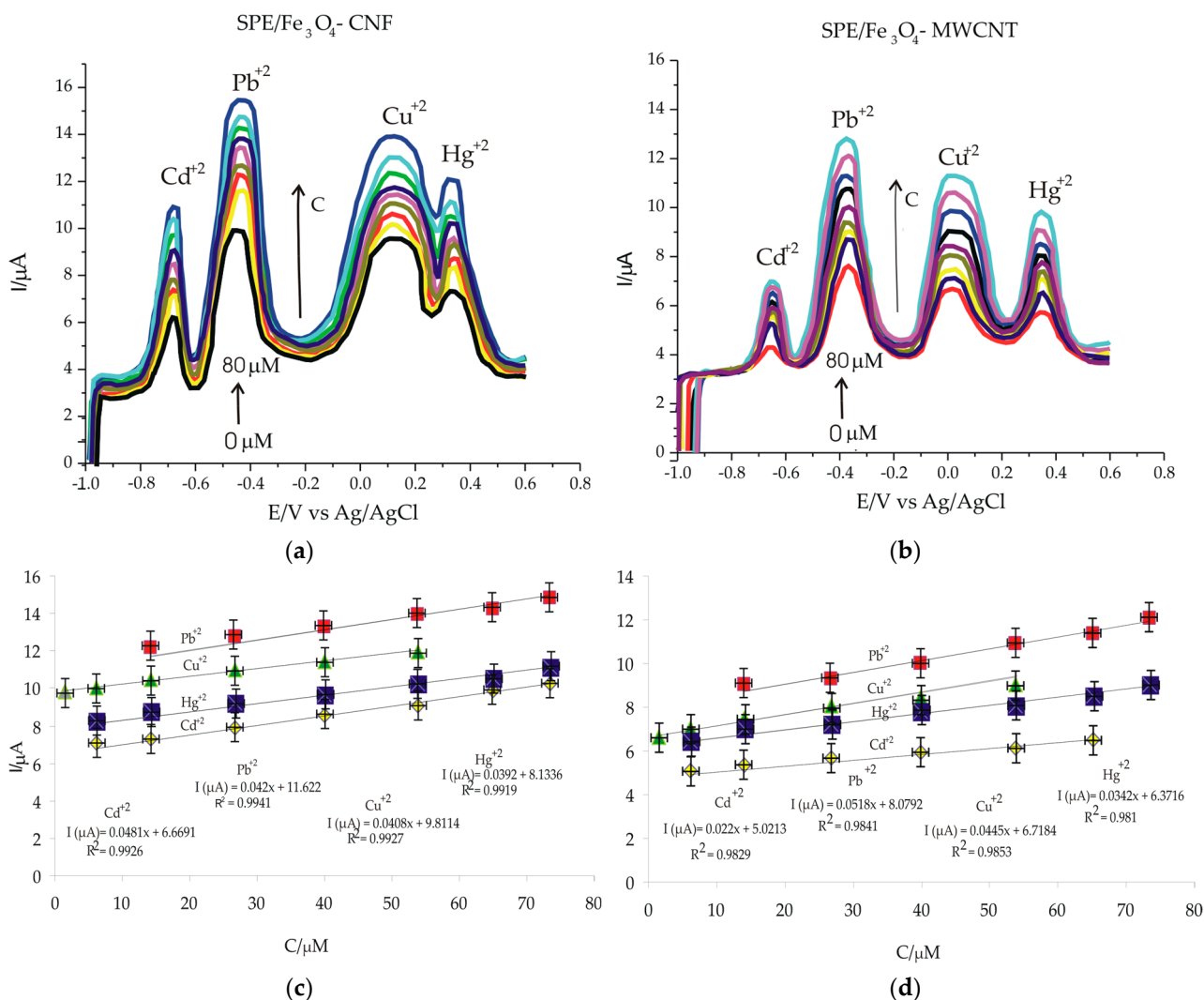
**Figure 8.** SWASV for (**a**) SPE/Fe$_3$O$_4$-CNF and (**b**) Fe$_3$O$_4$-MWCNT immersed in solutions containing the metal ions Cd$^{2+}$, Pb$^{2+}$, Cu$^{2+}$ and Hg$^{2+}$ at different concentrations: 0.5, 1.5, 5, 15, 25, 40, 55, 65, 75, 80 μM; The calibration curves and the equations of the calibration lines obtained by the electrodes (**c**) SPE/Fe$_3$O$_4$ -CNF and (**d**) Fe$_3$O$_4$-MWCNT.

The linear dependence between the intensity of the peaks and their concentration in solution led to obtaining some quality linear models with coefficients between 0.98 and 1. Using the calibration equations, limits of detection (LOD) were calculated based on the relation 3 υ/m, where υ is standard deviation and m is the slope value, and limit of quantification (LOQ) was calculated according to the relation 10 υ/m. All these obtained values are included in Table 4. Comparing the two sensors performed in this study, it can be appreciated that the SPE/Fe$_3$O$_4$-CNF sensor is more sensitive for the detection of the studied Cd$^{2+}$ and Hg$^{2+}$, with lower detection and quantification limits. The superior performance of SPE/Fe$_3$O$_4$-CNF is due to the synergistic interaction between carbon nanofibers and Fe$_3$O$_4$ nanoparticles, the increased adsorption rate on the modified surface of heavy metal cations in the presence of bismuth ions [63]. Furthermore, the thin and long fibers of CNF allow for uniform dispersion in the matrix, enhancing structural stability and homogeneous distribution among Fe$_3$O$_4$ nanoparticles. Additionally, the long fiber of CNF improves the mechanical strength of composite materials, providing superior properties compared to shorter carbon nanotubes. These characteristics contribute to a lower detection limit and an extended linear range in the sensor's performance.

Also, the sensors developed and characterized in this study were compared with other sensors reported in the literature for simultaneous detection of heavy metals $Cd^{2+}$, $Pb^{2+}$, $Cu^{2+}$ and $Hg^{2+}$. It is observed that the results obtained are comparable or even better than those obtained with other devices when detecting the same metal ions, as shown in Table 5.

**Table 5.** Comparative results of the performance of the electrodes reported in this study with those in the literature.

| Electrode Material | Metal Ion | Method | Linear Range (µM) | LOD (µM) | LOQ (µM) | Reference |
|---|---|---|---|---|---|---|
| SPE/Fe$_3$O$_4$-CNF | Cd$^{2+}$ | SWASV | 6–80 | 0.0615 | 0.2065 | In this study |
| | Pb$^{2+}$ | | 14–80 | 0.0154 | 0.0514 | |
| | Cu$^{2+}$ | | 1–60 | 0.0320 | 0.1066 | |
| | Hg$^{2+}$ | | 6–80 | 0.0148 | 0.0493 | |
| SPE/Fe$_3$O$_4$-MWCNT | Cd$^{2+}$ | SWASV | 6–70 | 0.2719 | 0.9064 | In this study |
| | Pb$^{2+}$ | | 14–80 | 0.3187 | 1.0623 | |
| | Cu$^{2+}$ | | 1–60 | 1.0436 | 3.4789 | |
| | Hg$^{2+}$ | | 6–80 | 0.9076 | 3.0256 | |
| SnO$_2$ modified electrode | Pb$^{2+}$ | SWASV | 0.3–0.1 | 0.0104 | 0.0259 | [79] |
| Fe$_3$O$_4$-chitosan modified GCE (glassy carbon electrode) | Cd$^{2+}$ | SWASV | 1.2–1.7 | 0.0392 | 0.1306 | [80] |
| | Pb$^{2+}$ | | 0.1–1.4 | 0.0422 | 0.1406 | |
| | Cu$^{2+}$ | | 0.3–1.2 | 0.0967 | 0.3223 | |
| | Hg$^{2+}$ | | 0.4–1.2 | 0.0957 | 0.3191 | |
| GCE/CN-polymer | Cd$^{2+}$ | DPASV | 0.04–0.27 | 2.27 | 7.56 | [81] |
| | Pb$^{2+}$ | | 0.002–0.15 | 0.8 | 2.66 | |
| Fe$_3$O$_4$@SiO$_2$ | Cd$^{2+}$ | DPASV | 0.1–100 | 0.0561 | 0.1871 | [82] |
| | Pb$^{2+}$ | | 0.1–80 | 0.0165 | 0.0550 | |
| | Cu$^{2+}$ | | 0.1–80 | 0.0794 | 0.2642 | |
| | Hg$^{2+}$ | | 0.1–100 | 0.0567 | 0.1891 | |

SWASV—square-wave anodic stripping voltammetry, DPASV—differential pulse anodic stripping voltammetry.

Since the SPE/Fe$_3$O$_4$-CNF sensor has shown superior analytical performance, it was used for the analysis of environmental samples, namely, water samples from the Danube River.

### 3.6. Studies on the Accuracy, Reproducibility and Stability of the SPE/Fe$_3$O$_4$-CNF Sensor

Studies on the accuracy and precision of the voltametric method were carried out in a solution of $Cd^{2+}$, $Pb^{2+}$, $Cu^{2+}$ and $Hg^{2+}$ containing the four cations in equal concentrations of $5 \times 10^{-6}$ M in $10^{-1}$ M acetate buffer solution of pH 5. Evaluation of the accuracy parameters was performed over a period of 10 consecutive days (inter-day) and also over a period of 1 day at different times at an interval of 3 h (intra-day). The relative standard deviation (RSD) obtained was reported in Table 6. Both short-term and long-term, good stability of Fe$_3$O$_4$-CNF electrode was found by the SWASV method, as the initial signal was preserved at 98.3% ($Cd^{2+}$), 95.24% ($Pb^{2+}$), 94.12% ($Cu^{2+}$) and 93.85% ($Hg^{2+}$), illustrated in Figure 9. The coefficients of variation are not lower than 5% and the results did not demonstrate significant differences between the anodic currents recorded on different days; this demonstrates the fact that the sensor is stable and can be used in electroanalysis.

**Table 6.** The recovery test of the electrode for accuracy and reproducibility of the method.

| Metallic Ion | | $Cd^{2+}$ | $Pb^{2+}$ | $Cu^{2+}$ | $Hg^{2+}$ |
|---|---|---|---|---|---|
| Accuracy (RSD%) | Intra-day | 2.05 | 2.19 | 2.87 | 2.42 |
| | Inter-day | 3.15 | 3.43 | 3.98 | 3.44 |
| Reproducibility (RSD%) | | 2.10 | 2.07 | 2.66 | 2.37 |
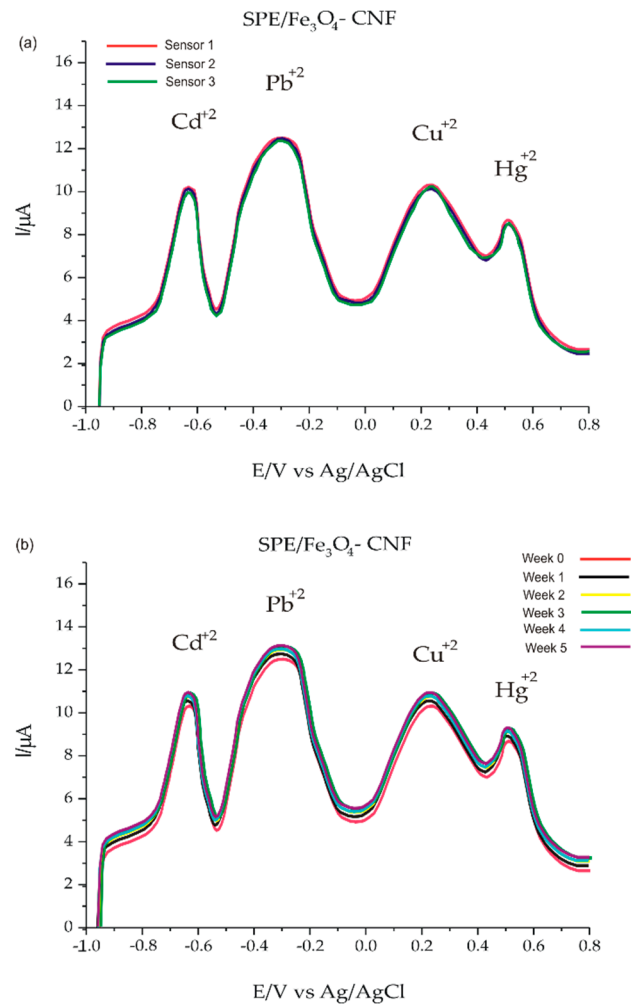


**Figure 9.** Reproducibility and stability measurements. (**a**) CV response of three SPE/Fe$_3$O$_4$-CNF prepared in similar conditions for the detection of $5 \times 10^{-6}$ M metal ions Cd$^{2+}$, Pb$^{2+}$, Cu$^{2+}$ and Hg$^{2+}$ in $10^{-1}$ M acetate buffer solution at pH 5; (**b**) the CV response of SPE/Fe$_3$O$_4$-CNF for the detection of $5 \times 10^{-6}$ M metal ions Cd$^{2+}$, Pb$^{2+}$, Cu$^{2+}$ and Hg$^{2+}$ in $10^{-1}$ M acetate buffer solution at pH 5 for five weeks.

The reproducibility of Fe$_3$O$_4$-CNF-modified sensor fabrication was studied in $5 \times 10^{-6}$ M Cd$^{2+}$, Pb$^{2+}$, Cu$^{2+}$ and Hg$^{2+}$ concentration solutions. Three identically constructed sensors on the same day were immersed in the solution to be analyzed. Therefore, the sensor fabrication process is suitable for obtaining sensors with analytical performance adequate for practical applications.

### 3.7. Interference Studies

Since some metal ions have a close reduction potential, it was considered in this study step to evaluate the selectivity of the SPE/Fe$_3$O$_4$-CNF sensor towards metal ions in complex

samples, where, in addition to the four metal ions studied, other metal ions such as $Co^{2+}$, $Ni^{2+}$, $Mn^{2+}$ and $Zn^{2+}$ were added.

There were insignificant changes in the peak currents of the studied ions in the presence of interfering ions. In this sense Figure 10 shows the voltammograms recorded in the presence of interfering ions $Co^{2+}$, $Ni^{2+}$, $Mn^{2+}$ and $Zn^{2+}$. The results obtained indicate variations in concentrations of less than 2% for all ions studied (Table 7).
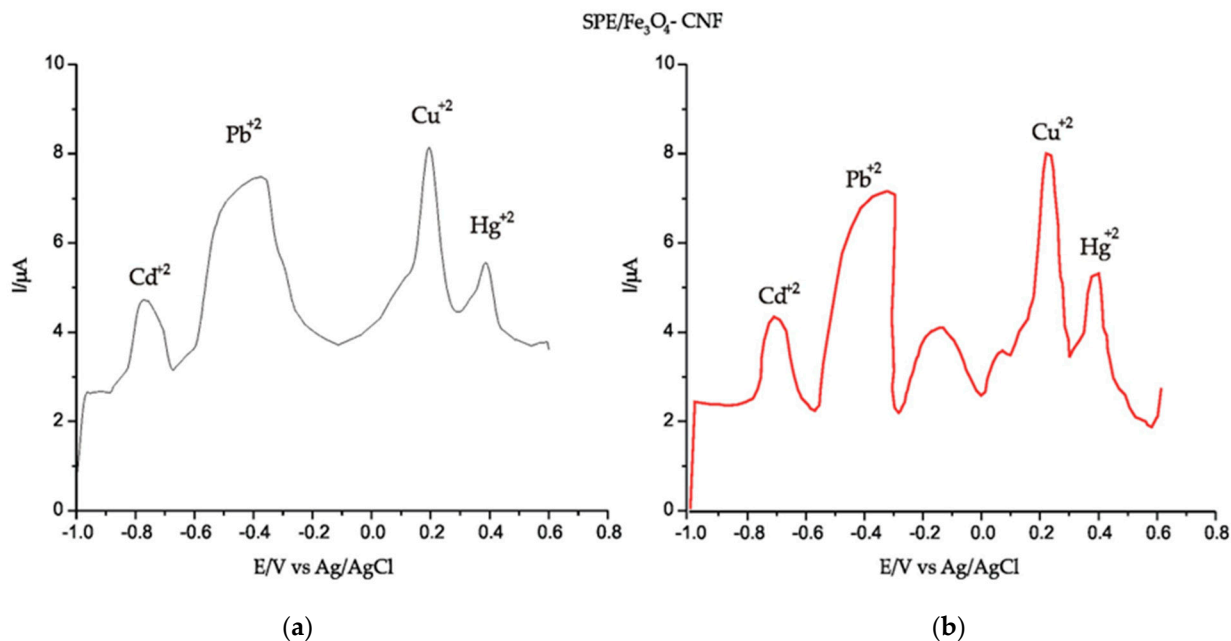


**Figure 10.** SWASV for SPE/Fe$_3$O$_4$-CNF immersed in solutions containing the metal ions $Cd^{2+}$, $Pb^{2+}$, $Cu^{2+}$ and $Hg^{2+}$ (**a**) and in solution with interfering ions $Co^{2+}$, $Ni^{2+}$, $Mn^{2+}$ and $Zn^{2+}$ (**b**) at concentration $2 \times 10^{-4}$ M in $10^{-1}$ M acetate buffer solution (pH 5.0).

**Table 7.** The results obtained for the quantitative determination of metal ions in the presence of interfering ions.

| Sample | [Cd$^{2+}$,Pb$^{2+}$, Cu$^{2+}$, Hg$^{2+}$]/M | [Co$^{2+}$,Ni$^{2+}$, Mn$^{2+}$, Zn$^{2+}$]/M | [Cd$^{2+}$,Pb$^{2+}$, Cu$^{2+}$, Hg$^{2+}$]/M Found | Recovery (RSD) (%) |
|---|---|---|---|---|
| | $2 \times 10^{-4}$ | $2 \times 10^{-4}$ | $2.01 \times 10^{-4}$ | $100.50 \pm 0.35$ |
| 1 | $3 \times 10^{-4}$ | $2 \times 10^{-4}$ | $3.02 \times 10^{-4}$ | $100.66 \pm 0.47$ |
| | $4 \times 10^{-4}$ | $2 \times 10^{-4}$ | $4.01 \times 10^{-4}$ | $100.25 \pm 0.17$ |
| | $5 \times 10^{-4}$ | $2 \times 10^{-4}$ | $5.01 \times 10^{-4}$ | $100.20 \pm 0.14$ |
| | $2 \times 10^{-4}$ | $3 \times 10^{-4}$ | $2.04 \times 10^{-4}$ | $102.00 \pm 1.4$ |
| 2 | $3 \times 10^{-4}$ | $3 \times 10^{-4}$ | $2.98 \times 10^{-4}$ | $99.33 \pm 0.47$ |
| | $4 \times 10^{-4}$ | $3 \times 10^{-4}$ | $3.99 \times 10^{-4}$ | $99.75 \pm 0.17$ |
| | $5 \times 10^{-4}$ | $3 \times 10^{-4}$ | $5.03 \times 10^{-4}$ | $100.60 \pm 0.42$ |
| | $2 \times 10^{-4}$ | $4 \times 10^{-4}$ | $2.02 \times 10^{-4}$ | $101.00 \pm 0.70$ |
| 3 | $3 \times 10^{-4}$ | $4 \times 10^{-4}$ | $3.04 \times 10^{-4}$ | $101.33 \pm 0.93$ |
| | $4 \times 10^{-4}$ | $4 \times 10^{-4}$ | $3.89 \times 10^{-4}$ | $97.25 \pm 1.97$ |
| | $5 \times 10^{-4}$ | $4 \times 10^{-4}$ | $4.95 \times 10^{-4}$ | $99.00 \pm 0.71$ |

**Table 7.** *Cont.*

| Sample | $[Cd^{2+}, Pb^{2+}, Cu^{2+}, Hg^{2+}]/M$ | $[Co^{2+}, Ni^{2+}, Mn^{2+}, Zn^{2+}]/M$ | $[Cd^{2+}, Pb^{2+}, Cu^{2+}, Hg^{2+}]/M$ Found | Recovery (RSD) (%) |
|---|---|---|---|---|
| 4 | $2 \times 10^{-4}$ | $5 \times 10^{-4}$ | $1.97 \times 10^{-4}$ | $98.50 \pm 1.06$ |
| | $3 \times 10^{-4}$ | $5 \times 10^{-4}$ | $3.06 \times 10^{-4}$ | $102.00 \pm 1.40$ |
| | $4 \times 10^{-4}$ | $5 \times 10^{-4}$ | $3.95 \times 10^{-4}$ | $98.75 \pm 0.88$ |
| | $5 \times 10^{-4}$ | $5 \times 10^{-4}$ | $5.01 \times 10^{-4}$ | $100.20 \pm 0.14$ |
| 5 | $2 \times 10^{-4}$ | $6 \times 10^{-4}$ | $2.03 \times 10^{-4}$ | $101.50 \pm 1.05$ |
| | $3 \times 10^{-4}$ | $6 \times 10^{-4}$ | $2.99 \times 10^{-4}$ | $99.66 \pm 0.23$ |
| | $4 \times 10^{-4}$ | $6 \times 10^{-4}$ | $3.94 \times 10^{-4}$ | $98.50 \pm 1.06$ |
| | $5 \times 10^{-4}$ | $6 \times 10^{-4}$ | $4.95 \times 10^{-4}$ | $99.00 \pm 0.71$ |

Analyzing these experimental results, it can be concluded that the SWASV method is suitable for the analysis of metal ions $Cd^{2+}$, $Pb^{2+}$, $Cu^{2+}$ and $Hg^{2+}$ in the presence of others, such as $Co^{2+}$, $Ni^{2+}$, $Mn^{2+}$ and $Zn^{2+}$.

### 3.8. Determination of Metal Ions in Water Samples

The applicability of the SPE/Fe$_3$O$_4$-CNF sensor was demonstrated by analyzing water samples taken from the Danube River from five different locations (Isaccea, Galati, Prut, Reni and Tulcea) on the same day.

The measurements with the developed sensor were performed by the SWASV method, using the same working parameters (f = 25 Hz, $E_{sw}$ = 20 V, $E_i$–$E_f$ = −1.0–0.6 V, absorption potential E = −1.2 V in 180 s and a desorption potential of 1 V in a time of 210 s) in order to quantify metal ions ($Cd^{2+}$, $Pb^{2+}$, $Cu^{2+}$ and $Hg^{2+}$), and, for each sample, we analyzed four replicates.

Figure 11a illustrates the voltammograms recorded with the SPE/Fe$_3$O$_4$-CNF sensor for the five water samples taken from different points.
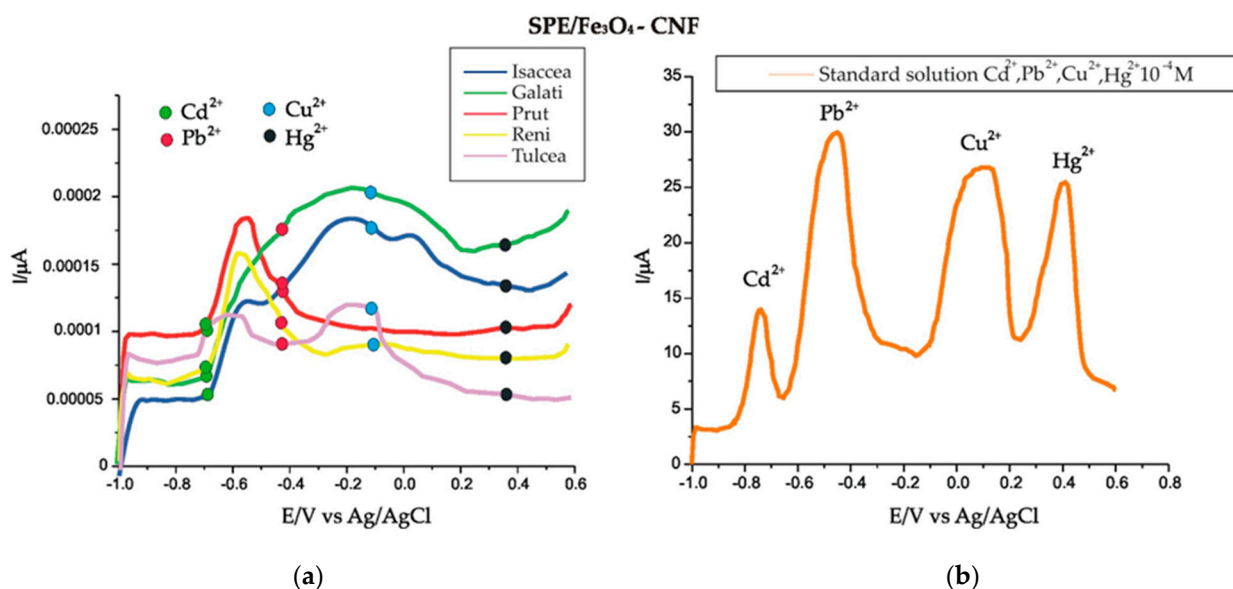


**Figure 11.** (**a**) SWASV of the SPE/Fe$_3$O$_4$-CNF sensor immersed in water samples taken on the same day from different points of the Danube River. (**b**) SWASV of the SPE/Fe$_3$O$_4$-CNF sensor immersed in standard solution $10^{-4}$ M $Cd^{2+}$, $Pb^{2+}$, $Cu^{2+}$ and $Hg^{2+}$ in $10^{-1}$ M acetate buffer solution (pH 5.0).

Using the measured anodic peak intensities at the specific potential of each metal ion and the equation of the calibration line, each concentration was calculated, as shown in Table 8.

**Table 8.** Heavy metal ion concentration values obtained with SPE/Fe$_3$O$_4$-CNF immersed in water samples taken on the same day from different points on the Danube River.

| Metals | C (µg/L) | | | | | USEPA [83] (µg/L) | WHO [83] (µg/L) |
|---|---|---|---|---|---|---|---|
| | Isaccea | Galati | Prut | Reni | Tulcea | | |
| Cd$^{2+}$ | 0.1171 | 0.1682 | 0.2360 | 0.1612 | 0.2827 | 5 | 3 |
| Pb$^{2+}$ | 0.6314 | 0.8633 | 0.8880 | 0.5525 | 0.4045 | 15 | 10 |
| Cu$^{2+}$ | 0.2337 | 0.2803 | 0.1541 | 0.1248 | 0.0967 | 1300 | 2000 |
| Hg$^{2+}$ | 0.7061 | 0.8289 | 0.5219 | 0.3689 | 0.2568 | 2 | 1 |

According to the intensity of the anodic peaks and the concentrations obtained for each metal ion (Table 8), the values fall within the maximum concentration limits laid out in currently enforced legislation. It can be emphasized that the SPE/Fe$_3$O$_4$-CNF sensor is sensitive to the detection of heavy metal ions included in this research and can be successfully used in surface water analysis.

### 3.9. Validation of Results by the Standard Addition Method

The sensor performance was validated using the standard addition method. Thus, in the already analyzed real samples (Isaccea), well-known concentrations of metal ions were added using $10^{-6}$ M standard solutions. The final concentrations of metal ions in the real samples were calculated, and the recoveries ranged between 96.89 and 103.41%, while the RSD (relative standard deviation) did not exceed 5%. These results indicate an optimal precision of the newly constructed sensor for detecting heavy metal ions in water samples. The results are presented in Table 9.

**Table 9.** Quantitative results obtained for the detection of metallic ions by the standard addition method.

| Sample | Cd$^{2+}$ (µg/L) Initial | Cd$^{2+}$ (µg/L) Added | Cd$^{2+}$ (µg/L) Found | Recovery (%) |
|---|---|---|---|---|
| | | 0.1 | 0.2221 | 102.30 ± 1.60 |
| | 0.1171 | 0.3 | 0.4061 | 97.36 ± 1.88 |
| | | 0.5 | 0.6211 | 100.64 ± 0.45 |
| | **Pb$^{2+}$ (µg/L) Initial** | **Pb$^{2+}$ (µg/L) Added** | **Pb$^{2+}$ (µg/L) Found** | **Recovery (%)** |
| | | 0.1 | 0.7421 | 101.46 ± 1.02 |
| | 0.6314 | 0.3 | 0.9025 | 96.89 ± 2.22 |
| | | 0.5 | 1.122 | 99.17 ± 0.58 |
| Isaccea | **Cu$^{2+}$ (µg/L) Initial** | **Cu$^{2+}$ (µg/L) Added** | **Cu$^{2+}$ (µg/L) Found** | **Recovery (%)** |
| | | 0.1 | 0.3451 | 103.41 ± 2.37 |
| | 0.2337 | 0.3 | 0.5301 | 99.32 ± 0.47 |
| | | 0.5 | 0.7425 | 101.19 ± 084 |
| | **Hg$^{2+}$ (µg/L) Initial** | **Hg$^{2+}$ (µg/L) Added** | **Hg$^{2+}$ (µg/L) Found** | **Recovery (%)** |
| | | 0.1 | 0.825 | 102.34 ± 1.63 |
| | 0.7061 | 0.3 | 1.026 | 101.97 ± 1.38 |
| | | 0.5 | 1.202 | 99.66 ± 0.24 |

The advantages of the prepared sensors are low cost, short preparation and result acquisition time, accuracy and portability for in situ sample measurement with minimal water sample treatment.

## 4. Conclusions

$Fe_3O_4$ nanoparticles with carbon nanofibers and multilayer carbon nanotubes were successfully synthesized and deposited on screen-printed carbon electrodes by the CA method. SPE/$Fe_3O_4$-CNF and SPE/$Fe_3O_4$-MWCNT sensors were prepared for the detection of heavy metal ions $Cd^{2+}$, $Pb^{2+}$, $Cu^{2+}$ and $Hg^{2+}$ both in standard solutions and in surface water samples. The best analytical performances were obtained with the SPE/$Fe_3O_4$-CNF sensor, compared to the SPE/$Fe_3O_4$-MWCNT sensor, by the SWASV method, a method with a series of advantages such as precision, reproducibility, stability, low cost and simplicity. Due to the fast response, low detection limit and good sensitivity, this sensor proves to be useful for the analysis of complex samples containing different heavy metal ions. All these positive aspects make this new sensor a promising monitoring tool for determining the quality of water or other environmental samples.

## References

1. Asrade, B.; Ketema, G. Determination of the Selected Heavy Metal Content and Its Associated Health Risks in Selected Vegetables Marketed in Bahir Dar Town, Northwest Ethiopia. *J. Food Qual.* **2023**, *2023*, 7370171. [CrossRef]
2. Bafe Dilebo, W.; Desta Anchiso, M.; Tereke Kidane, T.; Eskezia Ayalew, M. Assessment of Selected Heavy Metals Concentration Level of Drinking Water in Gazer Town and Selected Kebele, South Ari District, Southern Ethiopia. *Int. J. Anal. Chem.* **2023**, *2023*, 1524850. [CrossRef] [PubMed]
3. Demaku, S.; Aliu, A.; Sylejmani, D.; Ahmetaj, B.; Halili, J. Determination of Heavy Metals in Bee Honey as a Bioindicator in the Istog, Drenas and Kastriot Regions. *J. Ecol. Eng.* **2023**, *24*, 191–200. [CrossRef]
4. Nzitiri Bwala, M.; Sabiu Imam, T.; Umar Zungum, I. Determination of Heavy Metals Contamination on Smoked Fish Sold at Some Fish Markets in Borno State, Nigeria. *J. Chem. Health Risks* **2023**, *13*, 135–143. [CrossRef]
5. Goya-Heredia, A.V.; Zafra-Mejía, C.A.; Rondón-Quintana, H.A. Spatial Analysis of Heavy Metal Pollution in Road-Deposited Sediments Based on the Traffic Intensity of a Megacity. *Atmosphere* **2023**, *14*, 1033. [CrossRef]
6. Oladeji, O.M.; Kopaopa, B.G.; Mugivhisa, L.L.; Olowoyo, J.O. Investigation of Heavy Metal Analysis on Medicinal Plants Used for the Treatment of Skin Cancer by Traditional Practitioners in Pretoria. *Biol. Trace Elem. Res.* **2024**, *202*, 778–786. [CrossRef] [PubMed]
7. Singh, P.D.D.; Murthy, Z.V.P.; Kailasa, S.K. Environmental Sampling of Heavy Metals from Air, Water, and Soil Samples. In *ACS Symposium Series*; Verma, D.K., Verma, C., Mahish, P.K., Eds.; American Chemical Society: Washington, DC, USA, 2023; Volume 1456, pp. 137–165, ISBN 978-0-8412-9705-0.
8. Jin, M.; Yuan, H.; Liu, B.; Peng, J.; Xu, L.; Yang, D. Review of the Distribution and Detection Methods of Heavy Metals in the Environment. *Anal. Methods* **2020**, *12*, 5747–5766. [CrossRef] [PubMed]
9. Hailu, R.; Nibret, M. Determining Heavy Metal Concentrations and Physicochemical Properties in Wastewater. *Adv. Toxicol. Toxic. Eff.* **2023**, *7*, 1–7. [CrossRef]
10. Okewale, I.A.; Grobler, H. Assessment of Heavy Metals in Tailings and Their Implications on Human Health. *Geosystems Geoenviron.* **2023**, *2*, 100203. [CrossRef]
11. He, J.; Yang, Y.; Christakos, G.; Liu, Y.; Yang, X. Assessment of Soil Heavy Metal Pollution Using Stochastic Site Indicators. *Geoderma* **2019**, *337*, 359–367. [CrossRef]

12. Badeenezhad, A.; Soleimani, H.; Shahsavani, S.; Parseh, I.; Mohammadpour, A.; Azadbakht, O.; Javanmardi, P.; Faraji, H.; Babakrpur Nalosi, K. Comprehensive Health Risk Analysis of Heavy Metal Pollution Using Water Quality Indices and Monte Carlo Simulation in R Software. *Sci. Rep.* **2023**, *13*, 15817. [CrossRef] [PubMed]

13. Lancellotti, B.V.; Hensley, D.A.; Stryker, R. Detection of Heavy Metals and VOCs in Streambed Sediment Indicates Anthropogenic Impact on Intermittent Streams of the U.S. Virgin Islands. *Sci. Rep.* **2023**, *13*, 17238. [CrossRef] [PubMed]

14. Han, W.; Zhao, R.; Liu, W.; Wang, Y.; Zhang, S.; Zhao, K.; Nie, J. Environmental Contamination Characteristics of Heavy Metals from Abandoned Lead–Zinc Mine Tailings in China. *Front. Earth Sci.* **2023**, *11*, 1082714. [CrossRef]

15. López-Botella, A.; Sánchez, R.; Paul, R.; Aizpurua, J.; Gómez-Torres, M.J.; Todolí-Torró, J.-L. Analytical Determination of Heavy Metals in Human Seminal Plasma—A Systematic Review. *Life* **2023**, *13*, 925. [CrossRef] [PubMed]

16. Mahmood, B.S. Estimation of Heavy Metal Accumulation in Cardiac Tissue of Gallus Gallus Within Polluted Areas. *E3S Web Conf.* **2023**, *391*, 01129. [CrossRef]

17. Fu, Z.; Xi, S. The Effects of Heavy Metals on Human Metabolism. *Toxicol. Mech. Methods* **2020**, *30*, 167–176. [CrossRef] [PubMed]

18. Shahjahan, M.; Taslima, K.; Rahman, M.S.; Al-Emran, M.; Alam, S.I.; Faggio, C. Effects of Heavy Metals on Fish Physiology—A Review. *Chemosphere* **2022**, *300*, 134519. [CrossRef] [PubMed]

19. Dinake, P.; Motswetla, O.; Kereeditse, T.T.; Kelebemang, R. Assessment of Level of Heavy Metals in Cosmetics. *Toxicol. Res. Appl.* **2023**, *7*, 239784732311566. [CrossRef]

20. Mitra, S.; Chakraborty, A.J.; Tareq, A.M.; Emran, T.B.; Nainu, F.; Khusro, A.; Idris, A.M.; Khandaker, M.U.; Osman, H.; Alhumaydhi, F.A.; et al. Impact of Heavy Metals on the Environment and Human Health: Novel Therapeutic Insights to Counter the Toxicity. *J. King Saud. Univ. Sci.* **2022**, *34*, 101865. [CrossRef]

21. Begum, R.; Akter, R.; Dang-Xuan, S.; Islam, S.; Siddiky, N.A.; Uddin, A.A.; Mahmud, A.; Sarker, M.S.; Grace, D.; Samad, M.A.; et al. Heavy Metal Contamination in Retailed Food in Bangladesh: A Dietary Public Health Risk Assessment. *Front. Sustain. Food Syst.* **2023**, *7*, 1085809. [CrossRef]

22. Hama Aziz, K.H.; Mustafa, F.S.; Omer, K.M.; Hama, S.; Hamarawf, R.F.; Rahman, K.O. Heavy Metal Pollution in the Aquatic Environment: Efficient and Low-Cost Removal Approaches to Eliminate Their Toxicity: A Review. *RSC Adv.* **2023**, *13*, 17595–17610. [CrossRef]

23. Yadav, N.; Maurya, B.M.; Chettri, D.; Pooja; Pulwani, C.; Jajula, M.; Kanda, S.S.; Babu, H.W.S.; Elangovan, A.; Velusamy, P.; et al. Artificial Intelligence in Heavy Metals Detection: Methodological and Ethical Challenges. *Hyg. Environ. Health Adv.* **2023**, *7*, 100071. [CrossRef]

24. Malik, Y.; Ackakzai, W.; Mustafa, S.; Saddozai, S.; Akbar, A. Accumulation of Heavy Metals and Detection of Resistant-Associated Genes in Pseudomonas Aeruginosa in an Edible Catfish (*Wallago attu*) from Pat Feeder Canal, Pakistan. *Iran. J. Fish. Sci.* **2023**, *22*, 602–614.

25. Okyere, E.Y.; Adu-Boahen, K.; Boateng, I.; Dadson, I.Y.; Boanu, N.Y.; Kyeremeh, S. Analysis of Ecological Health Status of the Muni Lagoon: Evidence from Heavy Metal Content in Its Water and Fish Samples. *Geogr. Environ.* **2023**, *10*, e00115. [CrossRef]

26. Gong, T.; Liu, J.; Liu, X.; Liu, J.; Xiang, J.; Wu, Y. A Sensitive and Selective Sensing Platform Based on CdTe QDs in the Presence of l-Cysteine for Detection of Silver, Mercury and Copper Ions in Water and Various Drinks. *Food Chem.* **2016**, *213*, 306–312. [CrossRef]

27. Gupta, S.; Pandotra, P.; Gupta, A.P.; Dhar, J.K.; Sharma, G.; Ram, G.; Husain, M.K.; Bedi, Y.S. Volatile (As and Hg) and Non-Volatile (Pb and Cd) Toxic Heavy Metals Analysis in Rhizome of Zingiber Officinale Collected from Different Locations of North Western Himalayas by Atomic Absorption Spectroscopy. *Food Chem. Toxicol.* **2010**, *48*, 2966–2971. [CrossRef] [PubMed]

28. Astuti, D.; Awang, N.; Othman, M.S.B.; Kamaludin, N.F.B.; Meng, C.K.; Mutalazimah, M. Analysis of Heavy Metals Concentration in Textile Wastewater in Batik Industry Center. *Jppipa Pendidik. Ipa Fis. Biol. Kim.* **2023**, *9*, 1176–1181. [CrossRef]

29. Fahimah, N.; Salami, I.; Oginawati, K.; Yapfrine, S.; Supriatin, A.; Thaher, Y. Mapping and Identifying Heavy Metals in Water Use as Chemicals of Potential Concerns in Upper Watershed. *Glob. J. Environ. Sci. Manag.* **2023**, *9*, 765–788.

30. Ashraf, A.; Saion, E.; Gharibshahi, E.; Yap, C.K.; Kamari, H.M.; Elias, M.S.; Rahman, S.A. Distribution of Heavy Metals in Core Marine Sediments of Coastal East Malaysia by Instrumental Neutron Activation Analysis and Inductively Coupled Plasma Spectroscopy. *Appl. Radiat. Isot.* **2018**, *132*, 222–231. [CrossRef]

31. Froes, R.E.S.; Borges Neto, W.; Naveira, R.L.P.; Silva, N.C.; Nascentes, C.C.; Da Silva, J.B.B. Exploratory Analysis and Inductively Coupled Plasma Optical Emission Spectrometry (ICP OES) Applied in the Determination of Metals in Soft Drinks. *Microchem. J.* **2009**, *92*, 68–72. [CrossRef]

32. Klassen, A.; Fernandes, R.F.; De Oliveira, D.C.; Do Nascimento, M.P.; Borges, M.M.C.; De Oliveira, M.A.L.; Calixto, L.A.; Borges, K.B. Short-End Injection Capillary Electrophoresis and Multivariate Analysis for Simultaneous Determination of Heavy Metals in Passiflora Incarnata Tea. *IJERPH* **2022**, *19*, 15994. [CrossRef] [PubMed]

33. Onchoke, K.K.; Sasu, S.A. Determination of Hexavalent Chromium (Cr(VI)) Concentrations via Ion Chromatography and UV-Vis Spectrophotometry in Samples Collected from Nacogdoches Wastewater Treatment Plant, East Texas (USA). *Adv. Environ. Chem.* **2016**, *2016*, 3468635. [CrossRef]

34. Kaasalainen, H.; Stefánsson, A.; Druschel, G.K. Determination of Fe(II), Fe(III) and Fe total in Thermal Water by Ion Chromatography Spectrophotometry (IC-Vis). *Int. J. Environ. Anal. Chem.* **2016**, *96*, 1074–1090. [CrossRef]

35. Galinytė, D.; Balčiūnaitė-Murzienė, G.; Karosienė, J.; Morudov, D.; Naginienė, R.; Baranauskienė, D.; Šulinskienė, J.; Kudlinskienė, I.; Savickas, A.; Savickienė, N. Determination of Heavy Metal Content: Arsenic, Cadmium, Mercury, and Lead in Cyano-Phycocyanin Isolated from the Cyanobacterial Biomass. *Plants* **2023**, *12*, 3150. [CrossRef] [PubMed]

36. Oladeji, O.M.; Aasa, O.A.; Adelusi, O.A.; Mugivhisa, L.L. Assessment of Heavy Metals and Their Human Health Risks in Selected Spices from South Africa. *Toxicol. Rep.* **2023**, *11*, 216–220. [CrossRef] [PubMed]

37. Tarik, M.; Noureddine, E.; Ahmed, B.; Abdelkhalek, B.; Mohamed, M.; Majida, M.; Ilham, Z. Heavy Metals Analysis and Quality Evaluation in Drinking Groundwater around an Abandoned Mine Area of Ouichane (Nador's Province, Morocco). *J. Ecol. Eng.* **2023**, *24*, 118–127. [CrossRef]

38. Habila, M.A.; ALOthman, Z.A.; El-Toni, A.M.; Labis, J.P.; Soylak, M. Synthesis and Application of $Fe_3O_4@SiO_2@TiO_2$ for Photocatalytic Decomposition of Organic Matrix Simultaneously with Magnetic Solid Phase Extraction of Heavy Metals Prior to ICP-MS Analysis. *Talanta* **2016**, *154*, 539–547. [CrossRef] [PubMed]

39. Zárate-Quiñones, R.H.; Custodio, M.; Orellana-Mendoza, E.; Cuadrado-Campó, W.J.; Grijalva-Aroni, P.L.; Peñaloza, R. Determination of Toxic Metals in Commonly Consumed Medicinal Plants Largely Used in Peru by ICP-MS and Their Impact on Human Health. *Chem. Data Collect.* **2021**, *33*, 100711. [CrossRef]

40. Smirnova, S.V.; Samarina, T.O.; Ilin, D.V.; Pletnev, I.V. Multielement Determination of Trace Heavy Metals in Water by Microwave-Induced Plasma Atomic Emission Spectrometry after Extraction in Unconventional Single-Salt Aqueous Biphasic System. *Anal. Chem.* **2018**, *90*, 6323–6331. [CrossRef]

41. Ng, H.K.M.; Lim, G.K.; Leo, C.P. Comparison between Hydrothermal and Microwave-Assisted Synthesis of Carbon Dots from Biowaste and Chemical for Heavy Metal Detection: A Review. *Microchem. J.* **2021**, *165*, 106116. [CrossRef]

42. Adepoju, A.; Jalloh, A.; Femi-Adepoju, A. Heavy Metal Contaminants in Popularly-Consumed Vegetables of Freetown, Sierra Leone. *Eur. J. Nutr. Food Saf.* **2023**, *15*, 12–21. [CrossRef]

43. Durmuşkahya, C.; Alp, H.; Hortooğlu, Z.S.; Toktas, Ü.; Kayalar, H. X-ray Fluorescence Spectroscopic Determination of Heavy Metals and Trace Elements in Aerial Parts of *Origanum sipyleum* L. from Turkey. *Trop. J. Pharm. Res.* **2016**, *15*, 1013. [CrossRef]

44. Wan, M.; Hu, W.; Qu, M.; Tian, K.; Zhang, H.; Wang, Y.; Huang, B. Application of Arc Emission Spectrometry and Portable X-ray Fluorescence Spectrometry to Rapid Risk Assessment of Heavy Metals in Agricultural Soils. *Ecol. Indic.* **2019**, *101*, 583–594. [CrossRef]

45. Sciuto, E.L.; Petralia, S.; Van Der Meer, J.R.; Conoci, S. Miniaturized Electrochemical Biosensor Based on Whole-cell for Heavy Metal Ions Detection in Water. *Biotech. Bioeng.* **2021**, *118*, 1456–1465. [CrossRef] [PubMed]

46. Raril, C.; Manjunatha, J.G. Fabrication of Novel Polymer-Modified Graphene-Based Electrochemical Sensor for the Determination of Mercury and Lead Ions in Water and Biological Samples. *J. Anal. Sci. Technol.* **2020**, *11*, 3. [CrossRef]

47. Tajik, S.; Beitollahi, H.; Nejad, F.G.; Dourandish, Z.; Khalilzadeh, M.A.; Jang, H.W.; Venditti, R.A.; Varma, R.S.; Shokouhimehr, M. Recent Developments in Polymer Nanocomposite-Based Electrochemical Sensors for Detecting Environmental Pollutants. *Ind. Eng. Chem. Res.* **2021**, *60*, 1112–1136. [CrossRef] [PubMed]

48. Lavanya, J.; Srinivasan, R.; Varsha, M.V.; Gomathi, N. Review—Metal-Organic Frameworks Composites for Electrochemical Detection of Heavy Metal Ions in Aqueous Medium. *J. Electrochem. Soc.* **2022**, *169*, 047525. [CrossRef]

49. Wang, X.; Qi, Y.; Shen, Y.; Yuan, Y.; Zhang, L.; Zhang, C.; Sun, Y. A Ratiometric Electrochemical Sensor for Simultaneous Detection of Multiple Heavy Metal Ions Based on Ferrocene-Functionalized Metal-Organic Framework. *Sens. Actuators B Chem.* **2020**, *310*, 127756. [CrossRef]

50. Duoc, P.N.D.; Binh, N.H.; Hau, T.V.; Thanh, C.T.; Trinh, P.V.; Tuyen, N.V.; Quynh, N.V.; Tu, N.V.; Duc Chinh, V.; Thi Thu, V.; et al. A Novel Electrochemical Sensor Based on Double-Walled Carbon Nanotubes and Graphene Hybrid Thin Film for Arsenic(V) Detection. *J. Hazard. Mater.* **2020**, *400*, 123185. [CrossRef]

51. Lu, Z.; Zhao, W.; Wu, L.; He, J.; Dai, W.; Zhou, C.; Du, H.; Ye, J. Tunable Electrochemical of Electrosynthesized Layer-by-Layer Multilayer Films Based on Multi-Walled Carbon Nanotubes and Metal-Organic Framework as High-Performance Electrochemical Sensor for Simultaneous Determination Cadmium and Lead. *Sens. Actuators B Chem.* **2021**, *326*, 128957. [CrossRef]

52. Oularbi, L.; Turmine, M.; Salih, F.E.; El Rhazi, M. Ionic Liquid/Carbon Nanofibers/Bismuth Particles Novel Hybrid Nanocomposite for Voltammetric Sensing of Heavy Metals. *J. Environ. Chem. Eng.* **2020**, *8*, 103774. [CrossRef]

53. Bounegru, A.V.; Apetrei, C. Evaluation of Olive Oil Quality with Electrochemical Sensors and Biosensors: A Review. *Int. J. Mol. Sci.* **2021**, *22*, 12708. [CrossRef] [PubMed]

54. Dinu, A.; Apetrei, C. A Review of Sensors and Biosensors Modified with Conducting Polymers and Molecularly Imprinted Polymers Used in Electrochemical Detection of Amino Acids: Phenylalanine, Tyrosine, and Tryptophan. *Int. J. Mol. Sci.* **2022**, *23*, 1218. [CrossRef] [PubMed]

55. Zhang, Y.; Niu, Q.; Gu, X.; Yang, N.; Zhao, G. Recent Progress on Carbon Nanomaterials for the Electrochemical Detection and Removal of Environmental Pollutants. *Nanoscale* **2019**, *11*, 11992–12014. [CrossRef]

56. Chamjangali, M.A.; Kouhestani, H.; Masdarolomoor, F.; Daneshinejad, H. A Voltammetric Sensor Based on the Glassy Carbon Electrode Modified with Multi-Walled Carbon Nanotube/Poly(Pyrocatechol Violet)/Bismuth Film for Determination of Cadmium and Lead as Environmental Pollutants. *Sens. Actuators B Chem.* **2015**, *216*, 384–393. [CrossRef]

57. Hai, T.L.; Hung, L.C.; Phuong, T.T.B.; Ha, B.T.T.; Nguyen, B.-S.; Hai, T.D.; Nguyen, V.-H. Multiwall Carbon Nanotube Modified by Antimony Oxide ($Sb_2O_3$/MWCNTs) Paste Electrode for the Simultaneous Electrochemical Detection of Cadmium and Lead Ions. *Microchem. J.* **2020**, *153*, 104456. [CrossRef]

58. Hou, H.; Zeinu, K.M.; Gao, S.; Liu, B.; Yang, J.; Hu, J. Recent Advances and Perspective on Design and Synthesis of Electrode Materials for Electrochemical Sensing of Heavy Metals. *Energy Environ. Mater.* **2018**, *1*, 113–131. [CrossRef]

59. Liao, Y.; Li, Q.; Wang, N.; Shao, S. Development of a New Electrochemical Sensor for Determination of Hg(II) Based on Bis(Indolyl)Methane/Mesoporous Carbon Nanofiber/Nafion/Glassy Carbon Electrode. *Sens. Actuators B Chem.* **2015**, *215*, 592–597. [CrossRef]

60. Agnihotri, A.S.; Varghese, A.; Nidhin, M. Transition Metal Oxides in Electrochemical and Bio Sensing: A State-of-Art Review. *Appl. Surf. Sci. Adv.* **2021**, *4*, 100072. [CrossRef]

61. Liang, R.; Du, Y.; Xiao, P.; Cheng, J.; Yuan, S.; Chen, Y.; Yuan, J.; Chen, J. Transition Metal Oxide Electrode Materials for Supercapacitors: A Review of Recent Developments. *Nanomaterials* **2021**, *11*, 1248. [CrossRef]

62. Kim, M.; Yoo, J.; Kim, J. Quasi-Solid-State Flexible Asymmetric Supercapacitor Based on Ferroferric Oxide Nanoparticles on Porous Silicon Carbide with Redox-Active p-Nitroaniline Gel Electrolyte. *Chem. Eng. J.* **2017**, *324*, 93–103. [CrossRef]

63. Wu, W.; Jia, M.; Zhang, Z.; Chen, X.; Zhang, Q.; Zhang, W.; Li, P.; Chen, L. Sensitive, Selective and Simultaneous Electrochemical Detection of Multiple Heavy Metals in Environment and Food Using a Lowcost $Fe_3O_4$ Nanoparticles/Fluorinated Multi-Walled Carbon Nanotubes Sensor. *Ecotoxicol. Environ. Saf.* **2019**, *175*, 243–250. [CrossRef] [PubMed]

64. Yi, X.; He, J.; Guo, Y.; Han, Z.; Yang, M.; Jin, J.; Gu, J.; Ou, M.; Xu, X. Encapsulating $Fe_3O_4$ into Calcium Alginate Coated Chitosan Hydrochloride Hydrogel Beads for Removal of Cu (II) and U (VI) from Aqueous Solutions. *Ecotoxicol. Environ. Saf.* **2018**, *147*, 699–707. [CrossRef] [PubMed]

65. Zhu, W.; Saddam Khan, M.; Cao, W.; Sun, X.; Ma, H.; Zhang, Y.; Wei, Q. $Ni(OH)_2$/NGQDs-Based Electrochemiluminescence Immunosensor for Prostate Specific Antigen Detection by Coupling Resonance Energy Transfer with $Fe_3O_4@MnO_2$ Composites. *Biosens. Bioelectron.* **2018**, *99*, 346–352. [CrossRef] [PubMed]

66. Wu, W.; Li, Y.; Jin, J.; Wu, H.; Wang, S.; Ding, Y.; Ou, J. Sensing Nitrite with a Glassy Carbon Electrode Modified with a Three-Dimensional Network Consisting of $Ni_7S_6$ and Multi-Walled Carbon Nanotubes. *Microchim. Acta* **2016**, *183*, 3159–3166. [CrossRef]

67. Ba-Abbad, M.M.; Benamour, A.; Ewis, D.; Mohammad, A.W.; Mahmoudi, E. Synthesis of $Fe_3O_4$ Nanoparticles with Different Shapes Through a Co-Precipitation Method and Their Application. *JOM* **2022**, *74*, 3531–3539. [CrossRef]

68. Stegarescu, A.; Cabrera, H.; Budasheva, H.; Soran, M.-L.; Lung, I.; Limosani, F.; Korte, D.; Amati, M.; Borodi, G.; Kacso, I.; et al. Synthesis and Characterization of MWCNT-COOH/$Fe_3O_4$ and CNT-COOH/$Fe_3O_4$/NiO Nanocomposites: Assessment of Adsorption and Photocatalytic Performance. *Nanomaterials* **2022**, *12*, 3008. [CrossRef]

69. Wang, S.; Zhang, J.; Gharbi, O.; Vivier, V.; Gao, M.; Orazem, M.E. Electrochemical Impedance Spectroscopy. *Nat. Rev. Methods Primers* **2021**, *1*, 41. [CrossRef]

70. Mitran, R.-A.; Georgescu, D.; STĂNICĂ, N.; Matei, C.; Berger, D. Coating Magnetite Nanoparticles with Mesostructured Silica Shell of Different Pore Size and Geometry. *Rom. J. Mater./Rev. Romana Mater.* **2016**, *46*, 437–443.

71. Wu, L.; Ge, Z.; Li, W.; Chen, F.; Zhou, Z. Multi-Stimuli Responsive Composite for Heavy Metal Detection Based on Mesoporous Silica and Polyelectrolyte Brush. *Int. J. Electrochem. Sci.* **2020**, *15*, 740–757. [CrossRef]

72. Krans, N.A.; Ahmad, N.; Alloyeau, D.; De Jong, K.P.; Zečević, J. Attachment of Iron Oxide Nanoparticles to Carbon Nanofibers Studied by In-Situ Liquid Phase Transmission Electron Microscopy. *Micron* **2019**, *117*, 40–46. [CrossRef] [PubMed]

73. Munteanu, I.-G.; Apetrei, C. Electrochemical Determination of Chlorogenic Acid in Nutraceuticals Using Voltammetric Sensors Based on Screen-Printed Carbon Electrode Modified with Graphene and Gold Nanoparticles. *Int. J. Mol. Sci.* **2021**, *22*, 8897. [CrossRef] [PubMed]

74. Gaur, R. Morphology Dependent Activity of PbS Nanostructures for Electrochemical Sensing of Dopamine. *Mater. Lett.* **2020**, *264*, 127333. [CrossRef]

75. Laviron, E.; Roullier, L.; Degrand, C. A Multilayer Model for the Study of Space Distributed Redox Modified Electrodes. *J. Electroanal. Chem. Interfacial Electrochem.* **1980**, *112*, 11–23. [CrossRef]

76. Borrill, A.J.; Reily, N.E.; Macpherson, J.V. Addressing the Practicalities of Anodic Stripping Voltammetry for Heavy Metal Detection: A Tutorial Review. *Analyst* **2019**, *144*, 6834–6849. [CrossRef] [PubMed]

77. Wygant, B.R.; Lambert, T.N. Thin Film Electrodes for Anodic Stripping Voltammetry: A Mini-Review. *Front. Chem.* **2022**, *9*, 809535. [CrossRef] [PubMed]

78. Lee, S.; Oh, J.; Kim, D.; Piao, Y. A Sensitive Electrochemical Sensor Using an Iron Oxide/Graphene Composite for the Simultaneous Detection of Heavy Metal Ions. *Talanta* **2016**, *160*, 528–536. [CrossRef] [PubMed]

79. Hu, J.; Li, Z.; Zhai, C.; Zeng, L.; Zhu, M. Photo-Assisted Simultaneous Electrochemical Detection of Multiple Heavy Metal Ions with a Metal-Free Carbon Black Anchored Graphitic Carbon Nitride Sensor. *Anal. Chim. Acta* **2021**, *1183*, 338951. [CrossRef] [PubMed]

80. Huang, H.; Chen, T.; Liu, X.; Ma, H. Ultrasensitive and Simultaneous Detection of Heavy Metal Ions Based on Three-Dimensional Graphene-Carbon Nanotubes Hybrid Electrode Materials. *Anal. Chim. Acta* **2014**, *852*, 45–54. [CrossRef]

81. Ma, M.; Fang, L.; Zhao, N.; Huang, X.; Meng, D.; Pan, C.; Liu, J.; Liu, W. Simultaneous Detection of Heavy Metals in Solutions by Electrodeposition Assisted Laser Induced Breakdown Spectroscopy. *J. Laser Appl.* **2022**, *34*, 012021. [CrossRef]

82. Zhang, M.; Guo, W. Simultaneous Electrochemical Detection of Multiple Heavy Metal Ions in Milk Based on Silica-Modified Magnetic Nanoparticles. *Food Chem.* **2023**, *406*, 135034. [CrossRef] [PubMed]
83. Okpara, E.C.; Fayemi, O.E.; Wojuola, O.B.; Onwudiwe, D.C.; Ebenso, E.E. Electrochemical Detection of Selected Heavy Metals in Water: A Case Study of African Experiences. *RSC Adv.* **2022**, *12*, 26319–26361. [CrossRef] [PubMed]